Title: CXCL12 targets the primary cilium cAMP/cGMP ratio to regulate cell polarity during migration

Authors: Melody Atkins[1], Michèle Darmon[1], Fiona Roche[2], Xavier Nicol[2], Christine Métin[1,*]

Affiliations:

[1]INSERM UMR-S 1270 ; Institut du Fer à Moulin, Sorbonne Université ; F-75005 Paris, France

[2]Institut de la Vision, Sorbonne Université, INSERM, CNRS ; F-75012 Paris, France

[*] Corresponding author. Email: christine.metin@inserm.fr

Summary: Directed cell migration requires sustained cell polarisation. In migrating cortical interneurons, nuclear movements are directed towards the centrosome that organises the primary cilium signalling hub. Primary cilium-elicited signalling, and how it affects migration, remain however ill characterised. Here, we show that altering cAMP/cGMP levels in the primary cilium by buffering cAMP, cGMP or by locally increasing cAMP, influences the polarity and directionality of migrating interneurons, whereas buffering cAMP or cGMP in the apposed centrosome compartment alters their motility. Remarkably, we identify CXCL12 as a trigger that alters the ciliary cAMP/cGMP ratio to promote sustained polarity and directed migration. We thereby uncover cAMP/cGMP levels in the primary cilium as a major target of extrinsic cues and as the steering wheel of neuronal migration.

Keywords: primary cilium, cortical interneurons, migration, second messengers, cAMP, cGMP, cell polarity, nucleokinesis, compartmentation

Introduction

Neuronal migration represents a major phase of brain development and abnormal migration has been linked to several neurological and mental disorders. Cell migration is defined as a directed motility process, and neurons, which are highly polarised cells, often progress in a saltatory way sometimes called *migration by nucleokinesis* [1]. They first extend a long leading process in a permissive or attractive environment. The centrosome moves forward to a proximal region of this process, known as the dilatation or swelling compartment [2,3]. Thereafter, the nucleus dynamically translocates towards the centrosome and the nuclear and swelling compartments merge together, allowing a new cycle to start over. Interestingly, the centrosome is also known as the organiser of the primary cilium (PC), a small microtubule-based structure that extends at the surface of almost all vertebrate cells. Ciliogenesis first involves the docking of a modified mother centriole – the basal body – to the plasma membrane. Extension of the ciliary membrane and microtubule core – or axoneme – is then ensured by a process termed intraflagellar transport, which involves the molecular motor-based bidirectional transport of various ciliary components [4]. Despite the structural continuum between the centrosome basal body and the ciliary axoneme, a transition zone assembled at the base of the PC acts as a physical barrier separating the cytoplasm from the cilioplasm. Remarkably, the PC has been involved in the long distance migration of neural crest cells [5] and tangentially migrating interneurons [6,7]. Like the centrosome, the PC moves forward to the swelling compartment [6,8]. Moreover, the PC of migrating interneurons hosts membrane receptors for guidance cues known to instruct migration [7]. Although guidance receptors are generally assumed to collect information at the cell front to guide growth cones in the environment, their potential role in the regulation of neuronal migration when located at the opposite pole of the cell within the PC remains unexplored. Our lab showed that PC ablation in migrating interneurons prevents their reorientation towards their final target [6], but the mechanisms responsible for this abnormal migratory behaviour have not been identified.

Long considered as a vestigial organelle of little functional importance, the PC is the target organelle of a family of developmental disorders termed ciliopathies[9], and is now well established as an antenna-like signalling hub, concentrating many specialised signalling components [4,10], among which components of the Hedgehog (Hh), WNT, receptor tyrosine kinase, transforming growth factor β (TGF-β), or bone morphogenetic protein (BMP) pathways. Primary cilia are also specialised compartments for second messenger signalling, such as signalling through the cAMP [11–14] and cGMP cyclic nucleotides [15]. Neuronal primary cilia are no exception. They indeed harbour the AC3 adenylyl cyclase [16], which produces cAMP, various GPCRs, responsible for the inhibition or activation of adenylyl cyclase-mediated cAMP production [17], and some of the main cAMP downstream effectors, such as the PKA kinase [12,18]. Similarly, cGMP signalling components have been reported in the outer segment photoreceptor [19] or in ciliary compartments of *C. Elegans* neurons [20,21]. However, the physiological relevance of ciliary cAMP and cGMP signals in neurons is still lacking to complete the jigsaw, especially in a context of migration. Remarkably, some of the above-mentioned guidance cues – i.e., semaphorin and CXCL12 – required for accurate cortical interneuron migration have been reported to converge onto these second messengers in a PC-independent context [22–26]. This therefore opens the possibility of a role for PC-elicited cAMP and cGMP signals downstream of extracellular guidance cues in order to instruct cortical interneuron migration.

cAMP and cGMP function together during different biological processes, whether in a converging [27,28] or antagonising mode [29–32]. cGMP and cAMP for example exert an antagonistic effect on axono- versus dendritogenesis in hippocampal neurites [32], or on attraction versus repulsion in response to Netrin-1 in neuronal growth cones [31]. Of note, they have both been involved in cortical interneuron migration [22,23,33], but only independently of each other. Moreover, their role in migration has exclusively been assessed at the whole-cell level. This whole-cell approach is in contradiction with an increasing amount of data pointing at a subcellular segregation of cAMP and cGMP micro-domains in order to spatiotemporally

orchestrate various cellular responses [12,29,34,35]. The many mechanisms required for accurate migration may thus be spatially organised and integrated within separate and specific subcellular compartments.

Here, we addressed this conceptual challenge by tackling a technical one: the targeting of signalling molecules within subcellular structures. We have developed an innovative toolset allowing the specific and local modulation of cAMP or cGMP levels within the PC of migrating cortical interneurons. We first show that specific ciliary cAMP or cGMP buffering dysregulates the cell polarity and directed migration of *in vitro* migrating interneurons in an opposite manner. We further demonstrate that these phenotypes are specific to the PC, since targeting our scavengers to a neighbouring subcellular compartment, i.e., the centrosome, no longer affects cell polarity, but rather cell motility. Photo-activation experiments moreover reveal that increasing ciliary cAMP levels phenocopies ciliary cGMP buffering, suggesting a mechanism by which opposite ciliary second messenger levels induce opposite cell polarity regulation. Finally, by combining *in vitro* pharmacological and *ex vivo* approaches in grafted brain organotypic slices, we propose a new conceptual model in which the CXCL12 chemokine secreted by cortical progenitors – which promotes the highly directional tangential migration of interneurons *in vivo* – targets the ciliary cAMP/cGMP levels of cortical interneurons and functions as an ON/OFF switch to set their highly directional mode of migration.

Results

Buffering cGMP or cAMP in the PC affects the polarity of migrating cortical interneurons

In order to assess the role of cAMP or cGMP signals in the PC of migrating cortical interneurons, we buffered cGMP or cAMP signals locally and specifically within the PC of migrating cells. This was achieved by addressing genetically encoded chelators specific of cGMP [36] (SponGee) or cAMP [37,38] (cAMP Sponge) to the PC by fusion to the 5HT6 targeting sequence [11], which codes for a ciliary G protein-coupled receptor [7]. Scavengers were moreover fused to the mRFP reporter to assess their subcellular localisation (Fig. 1A). The mRFP-tagged 5HT6 sequence – devoid of any of the two sponges – was used as a control construct. All constructs were co-electroporated in MGE-derived cortical interneurons with a cytoplasmic GFP reporter to monitor cell morphology. Efficient PC targeting of the 5HT6-SponGee- and 5HT6-cAMP Sponge-encoded proteins was confirmed by co-localisation with the Arl13b marker in immunohistochemistry experiments (Fig. 1B-C).

Using an *in vitro* co-culture model previously established in the lab to analyse the motility and directionality of electroporated MGE-derived interneurons, we analysed the consequences of ciliary cGMP or cAMP buffering on such migratory behaviours. Electroporated E14.5 medial ganglionic eminence (MGE) explants were co-cultured and allowed to migrate on a substrate of dissociated cortical cells (Fig. 1D). Time-lapse confocal imaging was then performed as MGE-derived interneurons started to migrate out of their explant and onto the cortical substrate (Fig. 1E). In this well-characterised *in vitro* preparation [2,6] (Fig. 1D), control interneurons migrate along a pretty straight trajectory, in which changes of polarity and direction – although possible – remain marginal (Fig. 1D-E). We first sought to rule out a potential involvement of the previously described 5HT6 constitutive activity – leading to increased cAMP production via Gαs signalling [39,40] – in the directionality and motility parameters of electroporated MGE cells. The migration of 5HT6-electroporated MGE cells was thus compared to cells electroporated with a mutated form of the 5HT6 receptor, devoid of any constitutive activity (Gs-dead mutation; Zhang et al., 2006; Fig. 1E-F). Remarkably, the mean directionality ratios of migrating interneurons, as well as their mean migration speed, are unaffected between the two conditions (Fig. 1I-K), validating our approach and confirming that neither cell directionality nor motility are altered by the 5HT6 receptor.

We thus proceeded with the analysis of migratory behaviours when addressing the cGMP and cAMP scavengers to the PC of migrating cells via the 5HT6 receptor. Of note, neither of the two ciliary sponges prevents migration (Fig. 1G-H; Videos S1&S2). Compared to control cells, ciliary cGMP buffering reduces the mean directionality ratios at each time point (Fig. 1G, L-M), in association with a reduced duration of persistent migration compared to control cells (Fig. 1N), due to frequent changes in polarity (Video S1). As a direct consequence of such changes in polarity – and thereby in directionality –, the average migration speed is decreased compared to 5HT6-electroporated cells (Fig. 1O). By contrast, targeting cAMP Sponge to the PC leads to highly directional cells with increased directionality ratios at each time point compared to controls (Fig. 1H, P-Q; Video S2), and no change in the average migration speed (Fig. 1R).

Changes in cortical interneuron directionality during their journey to the developing cortex have been linked to changes in branching behaviours [22,23,41]. Two major branching mechanisms exist. While exploring their environment for guidance information, interneuron growth cones do not turn, but rather split, forming a dichotomised leading process. Only one of the two end branches is stabilised, while the other retracts before nucleokinesis, usually resulting in mild adjustments of the migration direction. Alternatively, new branches can be formed from the soma/swelling compartment, allowing the centrosome to select a new leading process in which the nucleus migrates, while the former leading process retracts. Since the nucleus-centrosome axis defines the cell polarity, this second branching mechanism induces drastic changes in polarity and migration direction, comprising polarity reversals. We thus analysed the branching phenotype of migrating cells by distinguishing branching events observed on the leading process or at the soma/swelling compartment (Fig. 1S). Our results show an

interaction in two-way anova tests between the genotype and branching compartment following the electroporation of either of the two ciliary-targeted scavengers (Fig. 1T-U). Ciliary cGMP buffering increases branching at the soma/swelling compartment compared to controls, while branching at the leading process is unchanged (Fig. 1T), which is coherent with reduced directionality ratios (Fig. 1L). Conversely, for ciliary cAMP buffering, branching at the soma is unchanged, while branching frequencies along the leading process decrease compared to controls (Fig. 1U), in agreement with more directional trajectories (Fig. 1P).

Taken together, our results show that buffering cGMP or cAMP at the PC of *in vitro* migrating cortical interneurons leads to an opposite dysregulation of cell polarity. While ciliary cGMP buffering induces frequent polarity reversals, ciliary cAMP buffering is responsible for a polarity maintenance phenotype.

Ciliary cGMP and cAMP-dependent migratory defects are specific to the PC compartment

We then asked the question of whether cAMP and cGMP signals regulate the same cellular function(s) at the centrosome and at the PC of migrating interneurons. Indeed, the PC and centrosome contribute to a functional unit made of two physically linked compartments that are nevertheless separated by a barrier, the transition zone (Fig. 2A).

To answer this question, we addressed SponGee and cAMP Sponge to the centrosome by fusion to the PACT targeting sequence [42] (Fig. 2A-C). Remarkably, and in contrast to PC targeting, both scavengers have the same effect on cortical interneuron migration when addressed to the centrosome. Compared to cells electroporated with the control PACT-mRFP construct – devoid of any sponge –, neither of the two scavengers (Fig. 2D-F) has an effect on cell directionality ratios (Fig. 2G-H, M-N) or on the duration of persistent migration (Fig. 2I,O). This suggests that unlike at the PC, cGMP or cAMP buffering at the centrosome does not have an effect on cell polarity. Unlike at the PC, the decreased migration speed we observe compared to controls (Fig. 2J,P) is therefore not a consequence of changes in polarity or direction. Further analyses show that in this case, decreased migration speed is linked to an increase in the mean duration of pauses (Fig. 2K,Q) and a decrease in the frequency of nucleokinesis (Fig. 2L,R;). Our results therefore support a model in which centrosome-located cGMP and cAMP signals regulate nucleokinesis during cortical interneuron migration, while regulating cell polarity when located within the PC subcellular compartment (Fig. S1).

To confirm the specificity of the phenotypes obtained when SponGee and cAMP Sponge are targeted to the PC or to the centrosome, we next investigated the potential impact of the sponges on cortical interneuron migration in the case of no targeting to any specific subcellular compartment (Fig. S2A). Of note, while SponGee and cAMP Sponge are expressed in the whole cytoplasm (Fig. S2B-F), the cilioplasm remains devoid of any expression of the non-targeted sponges, most likely due to the transition zone acting as a physical barrier at its base (Fig. S2B-C; Ros et al., 2020). No effect on cell directionality (Fig. S2G-H, J-K) or migration speed (Fig. S2I,L) is observed in the absence of any subcellular targeting of the scavengers. Without excluding additional effects of cytoplasmic second messengers on migration – by affecting cell morphology for example– our results suggest that cGMP and cAMP sponges need to be targeted to specific subcellular compartments of migrating cells to alter their directionality and migration speed. Whereas soluble scavengers are excluded from the cilioplasm due to the presence of a filtering zone at the base of the PC, the centrosomal targeting of the cytoplasmic scavengers could be minimal, given the highly organised and dense structure of the centrosome and its surrounding matrix revealed by super-resolution fluorescence imaging [44], and given the very close apposition of the Golgi apparatus to the centrosome [45] which could reduce the accessibility of soluble scavengers to the centrosome.

Increasing ciliary cAMP levels by photo-activation mimics the polarity defects induced by ciliary cGMP buffering

cGMP and cAMP signalling function together in many biological systems, and often oppose each other by regulating antagonistic functions. This could arise either as a consequence of their opposite regulation of common downstream effectors, or of their respective activation of distinct and opposing downstream signalling pathways [29,32,46]. An additional level of counteraction has been reported, by which the reciprocal cAMP/cGMP levels are negatively correlated to one another, with for example a cAMP increase associated to a cGMP reduction in several neuronal systems [30–32].

We thus wondered whether the opposite cell polarity phenotypes obtained by ciliary cGMP or cAMP buffering during migration could moreover rely on an opposite regulation of ciliary cAMP and cGMP levels. To address this question, we fused the light-sensitive adenylyl cyclase bPAC [37,47] to the 5HT6 sequence (Fig. 3A) and locally increased ciliary cAMP levels by photo-activation (Fig. 3B). Compared to control 5HT6-electroporated cells (Fig. 3C), 5HT6-bPAC electroporation and photo-activation (Fig. 3D) decreases the mean directionality ratios (Fig. 3E-F) and duration of persistent migration (Fig. 3G), as well as the average migration speed (Fig. 3H). Remarkably, theses three migratory defects are those associated with ciliary cGMP buffering and cell polarity reversals (Fig. 1G, L-O), by opposition to the cell polarity maintenance phenotype induced by ciliary cAMP buffering (Fig.1H, P-R).

Our results are thus compatible with a ciliary balance model in which ciliary cAMP and cGMP levels oppose each other (Fig. 3I), since increasing ciliary cAMP levels by photo-activation mimics the phenotype obtained by ciliary cGMP buffering. In agreement with this model, inverting the ciliary cAMP/cGMP ratio by switching from cAMP photo-activation to cAMP buffering is sufficient to switch the cell polarity phenotype from frequent to rare polarity reversals (Fig. 3I-J, Fig. S1).

CXCL12 modulates the respective cAMP and cGMP levels in the PC and controls cortical interneuron directionality within the deep tangential stream

In vivo, cortical interneurons enter the cerebral cortex by its lateral border and migrate tangentially towards the medial cortex in the deep proliferative subventricular zone (SVZ) and in the superficial marginal zone (MZ). At any location along the tangential streams, a proportion of interneurons can re-orient radially in order to leave the tangential paths and to integrate the cortical plate (CP). This "tangential-to-radial switch" of migration represents a major directional change operated by migrating cortical interneurons to reach their cortical target [48]. Among the guidance cues required for cortical interneurons to migrate in the embryonic cortex, the CXCL12 chemokine secreted by the MZ and by cortical progenitors in the SVZ/IZ (intermediate zone), promotes the cortical interneuron tangential migration within the deep and superficial tangential migratory streams through binding to the CXCR7 and CXCR4 receptors [22,23,49–51]. CXCL12 binding to CXCR4 has moreover been reported to induce a Gi-mediated inhibition of adenylyl cyclase and reduction in cellular cAMP levels, leading to increased migration speed, reduced branching and subsequent increased migration directionality within the tangential stream [22].

Here, we examined whether the CXCL12 effect on increased cortical interneuron directionality may be the result of a local CXCL12 effect at the PC. Corroborating this idea, our results show an increase in the directionality of migrating cells and a reduced branching at the leading process only in the case of ciliary cAMP buffering (Fig. 1P-Q,U). By contrast, cAMP buffering in the whole cytoplasm (Fig. S2 J-K,O) or locally at the centrosome (Fig. 2M-N) never leads to any changes in directionality or branching compared to controls. Moreover, the CXCR4 receptor for CXCL12 has been found in cortical interneuron primary cilia [7], in addition to its localisation at the leading process and soma [23].

To test our hypothesis, we first took advantage of our *in vitro* co-culture model to assess the influence of CXCL12 on the directionality and migration speed of cortical interneurons electroporated with constructs that specifically erase cAMP or cGMP signals in the PC. Confocal time lapse imaging was initiated as cells started their migration. CXCL12 was added to the culture medium after 5 hours and imaging continued for another 10 hours (Fig. 4A-C). Importantly, analysis of the migratory behaviours

of electroporated MGE cells prior to drug application reproduces the phenotypes obtained previously (Fig. 4B): while ciliary cAMP buffering increases directionality ratios (Fig. 4D,F; light grey and green curves and histogram bars) without affecting the average migration speed (Fig. 4G; light grey and green histogram bars), ciliary cGMP buffering reduces both directionality ratios (Fig. 4E-F; light grey and purple curves and histogram bars) and migration speed compared to controls (Fig. 4G; light grey and purple histogram bars). CXCL12 application on control 5HT6-electroporated cells (Fig. 4C, left sequence) increases directionality ratios (Fig. 4D-E,F; light and dark grey curves and histogram bars) to the same levels as those observed prior to drug application for MGE cells electroporated with 5HT6-cAMP Sponge (Fig. 4D,F; dark grey and light green curves and histogram bars). The mean migration speed of control cells is also increased by CXCL12 application (Fig. 4G), as previously observed [22]. CXCL12 therefore appears sufficient to convert the directionality of a "control-like" migrating cell to a "5HT6-cAMP Sponge-like" migratory behaviour. In agreement, CXCL12 application on cells electroporated with 5HT6-cAMP Sponge (Fig. 4C, middle sequence) maintains directionality ratios at the same high levels as observed prior to drug application (Fig. 4D,F; light and dark green curves and histogram bars). On the other hand, CXCL12 application on cells electroporated with 5HT6-SponGee (Fig. 4C, right sequence), which phenocopies cAMP production in the PC, is sufficient to switch directionality ratios from low – prior to drug application – to high (Fig. 4E, light and dark purple curves), reaching levels comparable to those induced by CXCL12 application on controls (Fig. 4E,F; dark purple and grey curves and histogram bars). CXCL12 application on 5HT6-SponGee-electroporated cells is therefore sufficient to convert the migration direction of a "5HT6-SponGee-like" cell to a "5HT6-cAMP Sponge-like" behaviour.

Given our *in vitro* results highlighting an effect of ciliary cGMP and cAMP signals on cell polarity/directionality (Fig. 1) and identifying CXCL12 as a chemoattractant that controls the directionality of migrating cells by regulating their ciliary cAMP/cGMP balance, we examined whether scavengers targeted to the PC (Fig. 5A) can control the tangential to radial switch of migrating interneurons within the cortical structure. Electroporated MGE explants were grafted at the subpallium/pallium boundary of E15.5 brain organotypic slices, a stage at which the embryonic cortex exhibits visible SVZ, ZI and CP layers (Fig. 5B). After 12 to16 hours culture, MGE-derived cortical interneurons exit the explant and start to migrate within the structured cortical substrate. Cells were left to migrate for an extra 48 hours before fixation. Due to the graft position in the host cortex, control cortical interneurons (Fig. 5C) exiting the grafted MGE start to migrate in a highly directional tangential stream within the VZ/SVZ regions boarding the ventricle, where CXCL12 is expressed [51,52]. During their tangential progression, interneurons re-orient themselves in the SVZ/IZ by extending a radially oriented leading process towards the developing CP. To assess the physiological role of PC-elicited second messenger signals on directional changes, we evaluated the tangential-to-radial orientation switch of MGE cells electroporated with PC-targeted scavengers within the SVZ of grafted cortical slices (Fig. 5D-E). The leading process angular orientation was measured as depicted in Fig. 5F and angles were categorised as low/tangential, intermediate or high/radial. Remarkably, while ciliary cAMP buffering increases the proportion of tangentially-oriented cells over the radial ones, ciliary cGMP buffering favours an increased leading process radial orientation, reflecting an increased radial migration switch towards the developing CP (Fig. 5G). Therefore, locally buffering cGMP of cAMP levels within the PC of *ex vivo* migrating cortical interneurons is sufficient to alter the tangential-to-radial migration switch occurring within the SVZ. Taken together, our results moreover highlight a strong coherence between the *in vitro* and *ex vivo* data. Indeed, both *in vitro* and *ex vivo* buffering of ciliary cGMP are responsible for polarity-driven changes in directionality, likely operated from the cell body compartment, while ciliary cAMP buffering maintains cell directionality and favours tangential migration.

Altogether, our results support a new conceptual model in which CXCL12 secreted by SVZ cortical progenitors binds to ciliary-located CXCR4 receptors on tangentially migrating MGE cells, thereby reducing ciliary cAMP levels. This stabilises the ciliary cAMP/cGMP balance in a conformation that

induces a cell polarity maintenance phenotype and a highly directional tangential migration mode (Fig. 6).

Discussion

Our study sheds light on a new signalling mechanism controlling the directionality of cortical interneuron migration that originates at the PC and involves a negative crosstalk between cGMP and cAMP signals. This newly-identified role for the PC as the steering wheel of cortical interneuron migration is independent of the cGMP- and cAMP-dependent cell motility process which is concomitantly regulated by the centrosome compartment. Finally, our results directly link the extracellular CXCL12 chemokine to PC-elicited second messengers, resulting in the precise regulation of the tangential-to-radial migration switch of cortical interneurons.

The PC signalling hub regulates cortical interneuron polarity via a ciliary cAMP/cGMP balance mechanism that opposes cAMP and cGMP downstream signalling

The PC is an evolutionary conserved organelle specialised in cAMP and cGMP signalling [15]. The strength of our approach relies on the specific manipulation of PC-located second messenger signals by combining the use of highly specific scavengers [36,37,38; Baudet et al., joined manuscript] and photo-activated constructs to their efficient targeting to the PC compartment via the 5HT6 sequence. Further validating our approach, compared to 5HT6 electroporation, electroporation of MGE cells with the 5HT6 receptor harbouring the Gs-dead mutation – known to abolish both the 5HT6 constitutive activity and the increased primary cilium length induced by 5HT6 overexpression [40,53] – does not affect cell directionality or migration speed, although the increased PC length is abolished (data not shown). The negative crosstalk we report between ciliary cGMP and cAMP signals is in line with other neuronal studies [29–32]. Although the mechanisms responsible for this opposition remain misunderstood, a reciprocal inhibition between each second messenger through phosphodiesterase-dependent hydrolysis has been proposed [32,46,54]. Our data are therefore compatible with a ciliary cAMP/cGMP balance mechanism in which high ciliary cAMP levels lead to PDE-dependent cGMP degradation, thereby inducing the same polarity reversal phenotype as ciliary cGMP buffering (Fig. 3).

A second level opposing ciliary cGMP and cAMP may arise from their respective activation of two distinct and opposing downstream signalling pathways, since buffering ciliary cGMP or cAMP impacts two distinct cellular compartments. While reduced ciliary cGMP signals may trigger a pathway that locally increases branching at the soma/swelling, reduced ciliary cAMP levels may lead to a signalling cascade reaching down to the leading process to inhibit branch formation and induce directional cell migration (Fig. 1). In both cases, the cytoskeleton is a likely downstream effector, especially since studies have already pointed it out as a downstream target of ciliary signals [55–57].

Cortical interneurons spatially organise additional cAMP and cGMP signalling compartments outside of the PC to regulate other aspects of migration

The ciliary cAMP/cGMP negative crosstalk regulating cell polarity is specific to the PC compartment, both functionally and mechanistically. Functionally, cGMP or cAMP buffering at the centrosome alters nucleokinesis, but not cell polarity. Moreover, unlike at the PC, we do not observe an opposition between cAMP and cGMP signals at the centrosome, since the buffering of either second messenger leads to the same dysregulation of nucleokinesis (Fig. 2). These results are in favour of a positive cAMP/cGMP crosstalk at the centrosome, with cAMP and cGMP signals converging on a pool of downstream effectors involved in a same process, rather than opposing each other. Such a positive crosstalk has already been observed in platelets [27,28], T-cells [58] or olfactory sensory neurons [59]. Our results are thus in line with several studies reporting the spatial segregation of cAMP and cGMP signals within different subcellular microdomains [12,29,34,35] and provide a concrete example of how cells may spatially organise such signals as well as their interplay to regulate different aspects of neuronal migration. Remarkably, another such example has also been evidenced during RGC axon guidance, in the lipid raft and non-lipid raft subcellular compartments (Baudet et al., joined manuscript). We here moreover confirm previous data reporting a deficient nucleokinesis associated with cAMP delocalisation from the

centrosome [60] (Fig. 2). Interestingly, although the centrosome had previously been described as a cAMP signalling centre during cell cycle progression or neuronal migration [60,61], its role in cGMP signalling had so far – to our knowledge – not been documented. Our study therefore brings new insight into the cAMP/cGMP interplay operating at this subcellular compartment.

The extracellular CXCL12 chemokine targets ciliary second messengers and acts as a switch to set a directional migration mode in the deep tangential stream

During development, CXCL12 mediates the directional tangential migration of cortical interneurons within the deep migratory stream, in a process involving a CXCR4-mediated decrease in cAMP levels [22,49]. Our results strongly suggest that the cAMP-dependent regulation of cell branching and directionality originates from a reduced ciliary cAMP activity – rather than a whole-cell decrease –, since an effect on either process was never observed with cAMP buffering in the whole cytoplasm (Fig. S2) or at the centrosome (Fig. 2). Of note, the reported effect of CXCL12 on increased migration speed – which we reproduce in our pharmacological experiments – is unlikely due to CXCL12 binding to the ciliary CXCR4 receptor, since we never observe increased migration speeds with any of our PC-targeted constructs. Alternatively, it could reflect the action of CXCR4-mediated cAMP decrease in another subcellular compartment outside of the PC. This further highlights the role of PC second messenger signalling as the steering wheel of migration, rather than its engine. We propose a model in which CXCL12 induces a "ciliary cAMP buffered-like" balance conformation leading to a highly directional migration mode in the SVZ (Fig. 6). Importantly, CXCL12 secretion by progenitor cells has been reported to decrease over time in a temporal pattern coinciding with the radial re-orientation of cortical interneurons towards the developing CP [62]. Conceptually, the ciliary cAMP/cGMP balance conformation switch that induces polarity changes and the radial re-orientation of migrating cells (Fig. 5) may therefore be triggered by switching off the CXCL12 signal: as CXCL12 expression decreases, ciliary cAMP levels may be allowed to increase, leading to a gradual inhibition of ciliary cGMP levels through PDE-mediated hydrolysis of ciliary cGMP [32]. We propose that switching off CXCL12 may lead to a ciliary cAMP/cGMP balance inversion favouring new branch formation towards the developing CP. This may in turn enable cells to respond to other extracellular molecules of the environment, such as the Shh morphogen, previously described to promote the tangential to radial switch of migrating cortical interneurons – in a yet undescribed mechanism.

Acknowledgments

This work was supported by the "Institut National de la Santé et de la Recherche Médicale" (INSERM), the "Agence Nationale de la Recherche" (ANR-18-CE16-0017, LocalHubs) and the "Ligue Nationale Contre le Cancer" (Subvention de Recherche Scientifique 2022). M.A. was supported by a two-year Young Investigator Grant from the Brain & Behavior Research Foundation and by a two-year postdoctoral fellowship from the Jerome Lejeune Foundation and the Sisley-d'Ornano Foundation.

We warmly thank the imaging platform of the "Institut du Fer à Moulin" for the use of their microscopes, as well as Pr. Fujio Murakami and Pr. Fumio Matsuzaki for their kind construct gifts. We are grateful to all members of the Métin team for their support and constructive discussions.

Author contributions

C.M. designed the study. M.A. performed the experiments and analysed the data. M.D, F.R. and X.N. designed the constructs. X.N. had insightful comments on the project and the manuscript. M.A. and C.M. wrote the manuscript.

Declaration of interests

The authors declare no competing interests.

Figure legends

Fig. 1: Specific buffering of ciliary cGMP or cAMP signals impairs cortical interneuron migratory behaviours in an opposite manner. (**A**) Representative scheme of a cortical interneuron PC, anchored to the centrosome via the mother centriole and physically separated from the cytoplasm by the transition zone. The mRFP-tagged SponGee or cAMP Sponge scavengers are fused to the 5HT6 sequence for PC targeting. (**B-C**) High magnification of cortical interneurons co-electroporated with a cytoplasmic GFP construct and 5HT6-SponGee (B) or 5HT6-cAMP Sponge (C). Immunostaining with anti-GFP, anti-RFP and anti-Arl13b antibodies revealed the efficient co-localisation of the mRFP-tagged sponges with the PC Arl13b marker. Insets are higher magnifications of the boxed region on the left. Scale bar, 5 μm; in insets, 1 μm. (**D**) Scheme of a MGE explant co-cultured on a dissociated cortical substrate. MGE-derived cortical interneurons show a characteristic saltatory migration pattern resulting in individual trajectories that radiate away from the explant of origin. (**E-H**) Time-lapse recordings of cortical interneurons co-electroporated with the GFP cytoplasmic construct and the control mRFP-tagged 5HT6 (E) and mut-5HT6 constructs (F), 5HT6-SponGee (G, see Video S1) or 5HT6-cAMP Sponge (H, see Video S2). Arrows and asterisks point at the dynamic mRFP-tagged PC and branch formation at the soma, respectively. Scale bar, 10 μm. (**I-R**) Mean directionality ratios at each time point (I,L,P) or after a maximum 350-minute migration period (J,M,Q), mean persistence duration (N) and mean migration speed (K,O,R) measured between the 5HT6 and the mut5HT6 (I-K), 5HT6-GSponGee (L-O) or 5HT6-cAMP Sponge conditions (P-R). (**S**) Schematics of branch quantification in (T,U). Leading process branches (green) initiate milder changes in direction (green arrow) than branches from the soma/swelling (pink; pink arrows). (**T-U**) Mean branching frequency from the soma/swelling and leading process compartments for 5HT6-SponGee- (T) and 5HT6-cAMP Sponge-electroporated cells (U) compared to 5HT6 controls. The number of cells is indicated below (J,K,M,N,O,Q,R) or on (T,U) graphs. *, $P \leq 0.05$; **, $P \leq 0.01$; ***, $P \leq 0.001$; ****, $P \leq 0.0001$, ns, non significant. Mann-Whitney test (J,K,M,N,O,Q,R). Two-way ANOVA test with Bonferroni's multiple comparison post test (T-U). (T) Interaction: ***; Genotype effect: **; Compartment effect: ****. (U) Interaction: **; Genotype effect: ns; Compartment effect: ****. Error bars are SEM.

Fig. 2: Buffering cGMP or cAMP at the centrosome of migrating cortical interneurons similarly dysregulates nucleokinesis without affecting cell polarity. (**A**) Representative scheme of the centrosome located in the cytoplasm at the base of the PC. The mRFP-tagged SponGee or cAMP Sponge scavengers are addressed to the centrosome by fusion to the PACT sequence. (**B-C**) High magnification of cortical interneurons co-electroporated with a cytoplasmic GFP construct and PACT-SponGee (B) or PACT-cAMP Sponge (C). Immunostaining with anti-GFP, anti-RFP and anti-γ-tubulin antibodies revealed the efficient co-localisation of the mRFP-tagged sponges with the centrosome. Insets are higher magnifications of the boxed region on the left. Scale bar, 5 μm; in insets, 1 μm. (**D-F**) Time-lapse recordings of cortical interneurons co-electroporated with the cytoplasmic GFP construct and the control mRFP-tagged PACT (D), PACT-SponGee (E) or PACT-cAMP Sponge (F). Arrows point at the mRFP-tagged centrosome. Scale bar, 10μm. (**G-R**) Mean directionality ratios at each time point (G,M), after a maximum 350- (H) or 300-minute migration period (N), mean persistence duration (I,O), mean migration speed (J,P) mean pause duration (K,Q) and mean number of translocations per hour (L,R) measured between the PACT and PACT-GSponGee (G-L) or PACT-cAMP Sponge (M-R) conditions. The number of cells is indicated below graphs (H,I,J,K,L,N,O,P,Q,R). **, $P \leq 0.01$, ****, $P \leq 0.0001$, ns, non significant. Mann-Whitney test (H,I,J,K,L,N,O,P,Q,R). Error bars are SEM.

Fig. 3: Increasing ciliary cAMP levels by photo-activation induces a polarity reversal phenotype. (**A**) Representative scheme of the cortical interneuron PC, anchored to the centrosome via the mother centriole and physically separated from the cytoplasm by the transition zone. The mRFP-tagged bPAC construct is targeted to the PC by fusion to the 5HT6 targeting sequence. (**B**) 5HT6-bPAC is photo-activated by blue light (491 nm laser) every minute for 2,1 seconds, leading to increased ciliary cAMP production. (**C-D**) Time-lapse recordings of cortical interneurons co-electroporated with the GFP

cytoplasmic construct and the control mRFP-tagged 5HT6 (C) or 5HT6-bPAC (D). Arrows and asterisks point at the dynamic mRFP-tagged PC and branch formation at the soma, respectively. Scale bar, 10 µm. (**E**) Graphical representation of the mean directionality ratios at each time point. (**F**). Mean directionality ratio after a maximum 350-minute migration period. (**G-H**) Mean persistence duration (G) and migration speed (H). (**I-J**) Hypothetical model depicting a ciliary cAMP/cGMP balance mechanism that regulates cortical interneuron polarity. Electroporation with 5HT6-bPAC or 5HT6-SponGee favours a ciliary balance conformation with higher cAMP levels compared to cGMP, and is associated with frequent polarity reversals (I). By contrast, inverting this ciliary cAMP/cGMP balance by electroporation of 5HT6-cAMP Sponge inverts the polarity phenotype from frequent to rare polarity reversals (and vice versa; J). The number of cells is indicated below graphs (E-H). **, $P \leq 0.01$, ****, $P \leq 0.0001$, ns, non significant. Mann-Whitney test (E-H). Error bars are SEM.

Fig. 4: CXCL12 bath application increases cell directionality in a way that mimics ciliary cAMP buffering. (**A**) Representative scheme of the *in vitro* protocol. MGE explants electroporated with 5HT6 (grey), 5HT6-SponGee (purple) and 5HT6-cAMP Sponge (green) are co-cultured on dissociated cortical cells. Live imaging starts as cortical interneurons initiate their migration and continues for 10 hours after CXCL12 is added to the culture medium. (**B-C**) Time-lapse recordings of cortical interneurons migrating in control medium (B) or after CXCL12 bath application (C). Interneurons were co-electroporated with the GFP cytoplasmic construct and the control mRFP-tagged 5HT6 (B-C, left-hand sequence), 5HT6-cAMP Sponge (B-C, middle) or 5HT6-SponGee (B-C, right-hand sequence). Arrows point at the dynamic mRFP-tagged PC. Scale bar, 10 µm. (**D-E**) Graphical representation of the mean directionality ratios at each time point over a 5-hour period, prior to (light curves) and after (dark curves) CXCL12 application, for the 5HT6 and 5HT6-cAMP Sponge conditions (D, grey and green curves, respectively) or for the 5HT6 and 5HT6-SponGee conditions (E, grey and purple curves, respectively). Directionality ratios are represented on two sets of graphs for more clarity, although MGE explants electroporated with each of the three scavengers were co-cultured on a same cortical substrate. Brown arrows highlight the increased directionality induced by 5HT6-cAMP Sponge electroporation or CXCL12 application, independently of the electroporated construct. (**F-G**) Mean directionality ratio after a maximum 5-hour migration period (F) and mean migration speed (G) for the 5HT6, 5HT6-cAMP Sponge and 5HT6-SponGee conditions prior to and after CXCL12 bath application. The number of cells is indicated below graphs. Statistically significant differences are reported using the * or # symbols, when comparing means to the 5HT6 condition or between non-control conditions, respectively. *, $P \leq 0.05$; **, $P \leq 0.01$; ***, $P \leq 0.001$; **** or ####, $P \leq 0.0001$. Two-way ANOVA test with Bonferroni's multiple comparison post test. (F) Interaction: ****; Genotype effect:****; Treatment effect:****. (E) Interaction: **; Genotype effect: ****; Treatment effect:****. Error bars are SEM.

Fig. 5: ciliary cGMP or cAMP buffering impairs the orientation of cortical interneurons migrating *ex vivo* in the SVZ. (**A**) Representative scheme of a cortical interneuron PC. The mRFP-tagged SponGee or cAMP Sponge chelators are fused to the 5HT6 sequence for PC targeting. (**B**) MGEs are dissected from E15.5 mouse embryos and co-electroporated with the cytoplasmic GFP construct and the desired scavenger. Electroporated MGEs are then grafted at the pallium-subpallium boundary of E15.5 organotypic slices and cells are left to migrate for 60 hours before fixation. Scale bar, 100 µm. (**C-E**) Epifluorescence acquisition of E15.5 brain organotypic slices grafted with MGEs co-electroporated with GFP and 5HT6 (C), 5HT6-SponGee (D) or 5HT6-cAMP Sponge (E). Slices were immunostained with the anti-RFP and anti-GFP antibodies. For clarity's sake, only the GFP staining is represented. SVZ/VZ, IZ and CP regions were delimitated using the dapi staining. Leading processes of migrating cells are drawn in green, purple or blue according to the value of their orientation angle (see F-G, below), namely tangential to the ventricle, radial or intermediate (respectively). Scale bar, 100 µm. (**F**) Representative scheme of the orientation angle (α) measured for each migrating cortical interneuron between the soma-swelling axis and the tangential to the ventricle. (**G**) α orientation angles were distributed in three categories corresponding to low (<30° or tangential orientation; green), high (>60° or radial orientation; purple) and intermediate angles (30°≤α<60°; blue). The number of cells is indicated on graphs.

Differential distribution of these angles was tested for 5HT6-cAMP Sponge- and 5HT6-SponGee-electroporated cells compared to controls using Chi-square tests. ****, $P \leq 0.0001$. SVZ, subventricular zone; VZ, ventricular zone; IZ, intermediate zone; CP, cortical plate; cIN, cortical interneuron.

Fig. 6: Summary and conclusive hypothetical model depicting the ciliary cAMP/cGMP switch activated by CXCL12 to set the tangential migration mode of cortical interneurons in SVZ. Within the SVZ, ventrally-born cortical interneurons (in green) are exposed to CXCL12 secreted by cortical intermediate progenitors. CXCL12 binds to the ciliary CXCR4 receptor of migrating cells, thereby inhibiting adenylyl cyclase-dependent cAMP production within the PC. The ciliary cAMP/cGMP balance is stabilised in a conformation with low ciliary cAMP levels compared to cGMP (Fig. 4, magnified PC in green), stabilising the polarity of migrating cells within the deep tangential stream, promoting sustained tangential migration. The proportion of tangentially oriented cells therefore increases compared to control cells, at the expense of radially oriented cells (Fig. 5). As CXCL12 expression decreases along time, adenylyl cyclase-dependent production of ciliary cAMP resumes gradually and ciliary cAMP levels increase, favouring a ciliary balance conformation with high cAMP levels compared to cGMP (magnified PC in purple). Cortical interneuron polarity is consequently unlocked and cortical interneurons extend new processes from the soma-swelling compartment, which can become new leading processes. The proportion of cells with radially oriented leading processes increases compared to controls (Fig. 5). CXCL12 expression is represented in brown as a decreasing gradient on the time axis. VZ, ventricular zone; SVZ, subventricular zone; IZ, intermediate zone; CP, cortical plate.

STAR Methods

Mice

Mouse embryos were collected from adult pregnant Swiss mice ordered from Janvier. Experiments were performed in the lab (Institut du Fer à Moulin, approval number D 75-05-22) in a conventional animal facility according to European guidelines. Experiments performed in the present study have been validated and approved by the Ethical committee Charles Darwin (C2EA-05, authorized projects 02241.02 and 29407).

Molecular biology

Control constructs

The pCX-5HT6-mCherry-GFP plasmid was a kind gift from the Nicol lab.
The pCAGGS-PACT-mKO1 and pCAGGS-PACT-GFP plasmids were kind gifts from Pr. Fumio Matsuzaki [42]. pCAGGS-eGFP was kindly gifted by Pr. Fujio Murakami.
Mut-5HT6-mRFP was generated by digestion of pCX-5HT6-mCherry-GFP with AgeI.
The mutated F69LT70ID72A 5HT6 sequence was generated using two rounds of PCR amplification with the Phusion DNA polymerase. First, we amplified the N-Ter moiety with 5HT6_for (5'- GGC AAAGAATTCTGATATCTTTAATCGCCACCATGGTT -3') and mut_5HT6_rev (5'-CACCAATCCCACC ATCAGGGCCGATATTAAGAGCGACACCAGGAAGAAG-3'), and the C-ter moiety using mut_5HT6_for (5'- CTTCTTCCTGGTGTCGCTCTTAATATCGGCCCTGATGGTGGGATTGGT-3') and 5HT6_rev (5'-GGAGCTAGCAACCGGTCCTCCTGC-3').
The purified N-ter end C-ter moieties were diluted, mixed and amplified with the Phusion DNA polymerase using 5HT6_mcherry_for (5'-TAATTAAACCCCGGGACCGGTGGATCCGG-3') and 5HT6_mCherry_rev (5'-CATGGTGGCGACCGGTCCTCCTG-3').
The full length mutated 5HT6 sequence was cloned using the infusion cloning system (Takara).
Non-targeted scavengers

The pCX-SponGee-mRFP and pCX-cAMP Sponge-mRFP plasmids were kind gifts from the Nicol lab.

Primary cilium-targeted constructs

pCX-5HT6-SponGee-mRFP was generated by digesting pCX-SponGee-mRFP with the restriction enzymes PacI and AgeI. 5HT6 was PCR-amplified from the pCX-5HT6-mCherry-GFP plasmid, using the CloneAmp HiFi PCR Premix (Ozyme, France; forward primer (5'-GGCAAAGAATTCTGATATCT TTAATCGCCACCATGGTT-3'); reverse primer (5'-GCTCCGGAGCTAGCAACCGGTCCTCCT-3').
pCX-5HT6-cAMP Sponge-mRFP was generated by digesting pCX-5HT6-SpiCee-mRFP [43] with the restriction enzymes BmtI and BglII. cAMP Sponge-mRFP was PCR-amplified from the pCDNA3-cAMP Sponge-mRFP plasmid, using the CloneAmp HiFi PCR Premix (Ozyme, France; forward primer (5'-AGGACCGGTTGCTAGGGCCATCTCCAAGA-3'); reverse primer (5'-TTTTGGCA GAGGGAAAAAGATCTAGGCGCCGGTGG-3').
Both plasmids were cloned using the NEBuilder HiFi DNA Assembly Cloning kit (New England Biolabs, UK).
pCX-5HT6-mRFP-bPAC was generated by digestion of pCX-LynLyn-mRFP (kind gift from the Nicol lab) with EcoRV and NotI. 5HT6 was PCR amplified from pCX-5HT6-SpiCee-mRFP-eGFP with the Phusion DNA Polymerase (NEB; forward primer: 5'-GCAAAGAATTCTGATGCCACCATGG TTCCAGAGC-3'; reverse primer: 5'-GAGGAGGCTGCGGCCGCACTGTTCATGGGGGAACCAAG-3').
The PCR fragment was cloned upstream of mRFP into pCX-LynLyn-mRFP-bPAC using the infusion cloning system (Takara)

Centrosome-targeted scavengers

pCX-PACT-SponGee was generated by digestion of pCX-5HT6-Spongee by AgeI and EcoRV.
pCX-PACT-cAMP Sponge was generated by digestion of pCX-5HT6-cAMP Sponge-mRFP by AgeI and EcoRV.
The 674bp PACT domain of mouse pericentrin, including a Kozak sequence upstream of the ATG initiation codon, was amplified from the pCAGGS-PACT-GFP plasmid (forward primer: 5'-GCAAAGAATTCTGATGCCACCATGGACCCAGAGTGGC-3'; reverse primer: 5'-GGAGCTAGCAACCGGCGACTGTTTAATCTTCTGGTG-3') using the Phusion DNA polymerase.
Both plasmids were cloned using the infusion cloning system (Takara).

Co-cultures and *in vitro* electroporation

Co-cultures were performed on polylysine/laminin-coated glass coverslips, either placed in culture wells or fixed to the bottom of perforated Petri dishes in order to image migrating MGE cells. Brains were collected in cold PBS at embryonic day E14.5. Cortices and MGE explants were then dissected in cold Leibovitz medium (Invitrogen). Cortices were mechanically dissociated. Dissociated cortical cells were cultured on the coated glass coverslips and left in the incubator (37°C, 5% CO2) during MGE electroporation. For electroporation, each MGE explant was placed in a small well of 3% agar. The desired constructs (described above) were diluted (1µg/µl or 0,7 µg/µl) with the pCAGGs-GFP construct (0,5 µg/µl or 0,4 µg/µl) in PBS with Fast Green added at a final concentration of 0,01%. The plasmid solution was micro-injected within the MGE explants using glass capillaries (Narishige, G-1.2). One pulse (100 V, 5 msec) was then delivered with a BTX electroporator using a petri dish equipped with electrodes (Nepagene, Sonidel, UE). Electroporated explants were then left to recover for at least one hour in F12/DMEM medium with 10% calf serum in the incubator (37°C, 5% CO2). Explants were then divided into smaller pieces and co-cultured on the dissociated cortical cells. MGE explants electroporated with a given construct were co-cultured on the same cortical substrate as MGE explants electroporated with the corresponding control construct to enable subsequent live imaging in the same conditions.

Brain organotypic slices

Organotypic slices were prepared from E15.5 embryonic brains embedded in 3% type VII agar (Sigma, A0701) and sectioned coronally using a manual slicer into 250 µm thick sections. Slices were then transferred onto Millicell chambers (Merck Millipore) for culture. After electroporation (as described above), E15.5 MGE explants were grafted in the cultured organotypic slices at the pallium/subpallium boundary. Grafted slices were then left to culture for 60 hours prior to fixation.

Pharmacology experiments

Recombinant mouse CXCL12 (Ref 460-SD-010, R&D systems, USA) was diluted in culture medium and applied on co-cultures after 5 hours of imaging by replacing half the volume of culture medium with the drug solution at 2,50 nM (final concentration of 1,25 nM).

Videomicroscopy

Time-lapse imaging was performed at 37°C with an inverted microscope (Leica DMI4000) equipped with a spinning disk (Roper Scientific, USA) and with a temperature-controlled chamber. The co-culture medium was replaced prior to acquisition with a culture medium of the same composition but without phenol red. Multi-position acquisition was performed with a Coolsnap HQ camera (Roper Scientific, USA) to allow the recording in the same conditions of MGE cells electroporated with a given construct or its corresponding control construct. Images were acquired with a x20 objective (LX20, Fluotar, Leica, Germany) and 491 nm and 561 nm lasers (MAG Biosystems, Arizona). Z-stacks of 7 µm were acquired with a step size of 1 µm every minute in the case of bPAC photo-activation or every 5 minutes for all other electroporated constructs, for up to 15 hours. A maximum of three experimental conditions (including the control condition) were imaged simultaneously, with a minimum of three positions

defined for each experimental condition. Acquisitions were controlled using the Metamorph software (Roper Scientific, USA).

Immunohistochemistry experiments

Co-cultures were fixed after 48 hours of culture in 4% PFA/ 0.33 M sucrose in 0.12M Phosphate Buffer for 15 minutes at room temperature. For γ-tubulin staining, co-cultures were fixed for 5 minutes at room temperature in 4% PFA/ 0.33 M sucrose in 0.12M Phosphate Buffer and then for 10 minutes at -20°C in 100% methanol. Organotypic slices were fixed by immersion in cold 4% PFA in 0.12M Phosphate Buffer for 3 hours and then pre-incubated for at least 5 hours in PGT (PBS; gelatin 2g/L; 0,25% Triton X-100).

Organotypic brain slices or co-cultures were then incubated overnight at 4°C in primary antibodies respectively diluted in PGT or PBT (PBS; 0.25% Triton X-100) with 2% normal goat serum and 1% bovine serum albumin (BSA, Sigma-Aldrich). After 3 rinses with PBT, brain sections or cells were incubated for 2h or 1h30 (respectively) with secondary antibodies diluted in PBT at 1/400. Brain sections were extensively washed in PBS after antibody incubation.

The following primary antibodies were used: chicken anti GFP (1/500, Aves Lab GFP-1020), rat anti RFP (1/1000, ChromoTek 5F8), rabbit anti Arl13b (1/500, Proteintech 17711-1-AP), mouse anti γ-tubulin (1/4000, Sigma T6557). Primary antibodies were revealed by immunofluorescence with the appropriate Alexa dye (Molecular Probes) or Cy3- and Cy5- conjugated secondary antibodies (Jackson laboratories) diluted in PBT (1/400). Bisbenzimide (1/5000 in PBT for 10 minutes (co-cultures) or 25 minutes (organotypic slices), Sigma) was used for nuclear counterstaining.

Co-cultures and brain organotypic slices were mounted in mowiol/DABCO (25mg/mL) and observed on a macroscope (MVX10 olympus) or on a LEICA DM6000 upright fluorescent microscope using an immersion x100 objective.

Image processing

For co-culture experiments, for each migrating cell, cell directionality ratios, as well as the mean migration speed, pause duration and number of translocations per hour were extracted from spinning disk acquisitions using the MTrackJ pluggin of ImageJ (NIH, USA) or the Metamorph software. Only cells co-electroporated with the construct of interest and the cytoplasmic GFP construct were taken into account for the analyses. Cells electroporated with only one of the two constructs – i.e., the PC-targeted sponge or the cytoplasmic GFP construct – were excluded from the analyses, in favour of co-electroporated cells. Directionality ratios are extracted for each cell at each migration time point and correspond to the ratio between the distance of the direct path the cell could have chosen and the distance of the real path it has followed. The duration of persistent migration corresponds to the average migration time spent by a cell without any change in polarity. Pauses were defined as the consecutive imaging time points with instant migration speeds (i.e., occurring between two imaging frames) below 25 µm/h. Mean pause duration corresponds to the mean of all the pausing periods displayed by a cell during its entire migration sequence. For each migrating cell, a translocation event was defined for each instant migration speed with a value higher or equal to 120 µm/h. The frequency of nucleokinesis was defined for each cell as the ratio between the number of translocation events and the time spent by the cell in migration. Average values obtained from three independent experiments for each individual cell were used for statistical analyses.

For *ex vivo* brain organotypic slice experiments, DAPI staining allowed to distinguish between the VZ/SVZ, IZ and CP regions. The proportion of cells co-electroporated with the PC-targeted scavengers and the cytoplasmic GFP construct was estimated around 90 %. On this basis, analyses were carried out on GFP-positive cells. Leading process orientation was extracted using ImageJ (NIH, USA). Angles

obtained from the different slices of four (control 5HT6 condition) or five (5HT6-CAMP Sponge and 5HT6-SponGee conditions) embryonic brains were used for statistical analyses.

Statistical analyses

All data were obtained from at least three independent experiments and are presented as mean ± SEM. (standard error of mean). Statistical analyses were performed with the GraphPad Prism software. Statistical significance of the data was evaluated using the unpaired two-tailed *t* test, the Mann–Whitney test, the Chi2 test or the Two-way ANOVA test followed by a Bonferroni post-hoc test. Data distribution was tested for normality using the D'Agostino and Pearson omnibus normality test. Values of $p<0.05$ were considered significant. In figures, levels of significance were expressed by * (or #) for $p<0.05$, ** (or ##) for $p<0.01$, *** (or ###) for $p<0.001$ and **** (or ####) for $p<0.0001$.

Supplemental information

Fig. S1: Summary diagram depicting the migratory phenotypes associated with cAMP or cGMP buffering at the centrosome or at the PC compartment. Migrating cortical interneurons electroporated with the control constructs (top panel) rhythmically alternate over time between phases of pause and nucleokinesis in a saltatory mode. Two events of nucleokinesis are depicted on the diagram, each represented by the induced displacement vector (thin arrow). The thick arrow represents the sum of each individual displacement vector. When the cAMP or cGMP scavengers are targeted to the centrosome (middle panel), the polarity of the cell (defined by the nucleus-swelling axis) is unchanged, but the frequency of nucleokinesis is reduced, resulting in increased pausing times and reduced migration speed. For the same amount of time, only one nucleokinesis event occurs and the final displacement vector is shorter compared to controls, although its directionality is unchanged. Finally, when the scavengers are addressed to the PC (bottom panel), ciliary cAMP or cGMP buffering induces opposite phenotypes on cell polarity and directionality. Ciliary cAMP buffering induces migrating cells to maintain their polarity (i.e., the centrosome moves forward and nucleokinesis occurs within the same leading process) and to reduce branching events at the leading process, resulting in increased directionality. The migration speed is unchanged compared to controls, as highlighted by the same frequency of nucleokinesis events and the final displacement vector, which is of equal length and directionality compared to the control situation. By contrast, cGMP buffering at the PC induces more branching at the soma compartment and frequent changes in cell polarity (i.e., the centrosome moves from one leading process to a newly-formed branch that becomes the new leading process), which results in a decreased directionality and migration speed. As a result, the final displacement vector is not only shorter compared to controls, but it is also inverted.

Fig. S2: Expression of the SponGee or cAMP Sponge scavengers in the whole cytoplasm does not affect cortical interneuron directionality or motility. (**A**) Representative scheme of a cortical interneuron and its PC. The mRFP-tagged SponGee or cAMP Sponge scavengers lacking the 5HT6-targeting sequence are addressed to the whole cytoplasm – excluding the cilioplasm. (**B-C**) High magnification of cortical interneurons co-electroporated with a cytoplasmic GFP construct and the SponGee (B) or cAMP Sponge (C) chelators. Cells were immunostained with anti-GFP, anti-RFP and anti-Arl13b antibodies. Notably, when addressed to the whole cytoplasm, the SponGee and cAMP Sponge scavengers fail to enter the Arl13b-positive PC. Insets are higher magnifications of the boxed region on the left. Dotted lines delimitate the border between cytoplasm and cilioplasm. Scale bar, 5 µm; in insets, 1 µm. (**D-F**) Time-lapse recordings of cortical interneurons co-electroporated with the GFP cytoplasmic construct and the RFP control construct (the tag without the sponge; D), SponGee (E) or cAMP Sponge (F). Scale bar, 10 µm. (**G**) Graphical representation of the mean directionality ratios at each time point for the RFP and SponGee conditions. (**H**) Mean directionality ratio after a maximum 350-minute migration period. (**I**) Mean migration speed. (**J**) Graphical representation of the mean directionality ratios at each time point for the RFP and cAMP Sponge conditions. (**K**) Mean directionality ratio after a 350-minute migration period. (**L**) Mean migration speed. (**M**) Schematics of branch quantification in (N,O). Leading process branches (green) initiate milder changes in direction (green arrow) than branches from the soma/swelling compartment (pink; pink arrows). (**N-O**) Mean branching frequency from the soma/swelling and leading process compartments for SponGee- (N) and cAMP Sponge-electroporated cells (O) compared to RFP controls. Quantifications were extracted from three independent experiments. The number of cells is indicated below (H,I,K,L) or on (N,O) graphs. P ≤ 0.001; ****; ns, non significant. Mann-Whitney test (H,I,K,L). Two-way ANOVA test with Bonferroni's multiple comparison post test (N) Interaction: ns; Genotype effect: ns; Compartment effect: ****. (O) Interaction: ns; Genotype effect: ns; Compartment effect: ****. Error bars are SEM.

Video S1: Ciliary cGMP buffering favours a cell polarity reversal phenotype *in vitro*. MGE-derived cortical interneuron co-electroporated with the cytoplasmic GFP construct and the mRFP-tagged 5HT6-GSponGee scavenger. A mRFP-positive PC is dynamically extended and retracted by the migrating

interneuron as it migrates, as highlighted by the white arrowhead. Remarkably, the migrating cell undergoes a polarity reversal that is reflected by a reversal in the direction of migration. Time interval between frames, 5 minutes (3 frames per second).

Video S2: Ciliary cAMP buffering favours a cell polarity maintenance phenotype *in vitro*. MGE-derived cortical interneuron co-electroporated with the cytoplasmic GFP construct and the mRFP-tagged 5HT6-cAMP Sponge scavenger. A mRFP-positive PC is dynamically extended and retracted by the migrating interneuron as it migrates, as highlighted by the white arrowhead. The migrating cell maintains its polarity (successive translocation cycles occur within the same leading process), resulting in a highly directional migration behaviour. Time interval between frames, 5 minutes (3 frames per second).

References (61)

1. Tsai, L.-H., and Gleeson, J.G. (2005). Nucleokinesis in neuronal migration. Neuron *46*, 383–388. 10.1016/j.neuron.2005.04.013.

2. Bellion, A., Baudoin, J.-P., Alvarez, C., Bornens, M., and Métin, C. (2005). Nucleokinesis in tangentially migrating neurons comprises two alternating phases: forward migration of the Golgi/centrosome associated with centrosome splitting and myosin contraction at the rear. J Neurosci *25*, 5691–5699. 10.1523/JNEUROSCI.1030-05.2005.

3. Schaar, B.T., and McConnell, S.K. (2005). Cytoskeletal coordination during neuronal migration. Proceedings of the National Academy of Sciences *102*, 13652–13657. 10.1073/pnas.0506008102.

4. Nachury, M.V., and Mick, D.U. (2019). Establishing and regulating the composition of cilia for signal transduction. Nat Rev Mol Cell Biol *20*, 389–405. 10.1038/s41580-019-0116-4.

5. Tobin, J.L., Di Franco, M., Eichers, E., May-Simera, H., Garcia, M., Yan, J., Quinlan, R., Justice, M.J., Hennekam, R.C., Briscoe, J., et al. (2008). Inhibition of neural crest migration underlies craniofacial dysmorphology and Hirschsprung's disease in Bardet-Biedl syndrome. Proc Natl Acad Sci U S A *105*, 6714–6719. 10.1073/pnas.0707057105.

6. Baudoin, J.-P., Viou, L., Launay, P.-S., Luccardini, C., Espeso Gil, S., Kiyasova, V., Irinopoulou, T., Alvarez, C., Rio, J.-P., Boudier, T., et al. (2012). Tangentially migrating neurons assemble a primary cilium that promotes their reorientation to the cortical plate. Neuron *76*, 1108–1122. 10.1016/j.neuron.2012.10.027.

7. Higginbotham, H., Eom, T.-Y., Mariani, L.E., Bachleda, A., Hirt, J., Gukassyan, V., Cusack, C.L., Lai, C., Caspary, T., and Anton, E.S. (2012). Arl13b in primary cilia regulates the migration and placement of interneurons in the developing cerebral cortex. Dev. Cell *23*, 925–938. 10.1016/j.devcel.2012.09.019.

8. Matsumoto, M., Sawada, M., García-González, D., Herranz-Pérez, V., Ogino, T., Nguyen, H.B., Thai, T.Q., Narita, K., Kumamoto, N., Ugawa, S., et al. (2019). Dynamic Changes in Ultrastructure of the Primary Cilium in Migrating Neuroblasts in the Postnatal Brain. J. Neurosci. *39*, 9967–9988. 10.1523/JNEUROSCI.1503-19.2019.

9. Reiter, J.F., and Leroux, M.R. (2017). Genes and molecular pathways underpinning ciliopathies. Nat Rev Mol Cell Biol *18*, 533–547. 10.1038/nrm.2017.60.

10. Nishimura, Y., Kasahara, K., Shiromizu, T., Watanabe, M., and Inagaki, M. (2019). Primary Cilia as Signaling Hubs in Health and Disease. Advanced Science *6*, 1801138. 10.1002/advs.201801138.

11. Jiang, J.Y., Falcone, J.L., Curci, S., and Hofer, A.M. (2019). Direct visualization of cAMP signaling in primary cilia reveals up-regulation of ciliary GPCR activity following Hedgehog activation. Proceedings of the National Academy of Sciences *116*, 12066–12071. 10.1073/pnas.1819730116.

12. Truong, M.E., Bilekova, S., Choksi, S.P., Li, W., Bugaj, L.J., Xu, K., and Reiter, J.F. (2021). Vertebrate cells differentially interpret ciliary and extraciliary cAMP. Cell *184*, 2911-2926.e18. 10.1016/j.cell.2021.04.002.

13. Sherpa, R.T., Mohieldin, A.M., Pala, R., Wachten, D., Ostrom, R.S., and Nauli, S.M. (2019). Sensory primary cilium is a responsive cAMP microdomain in renal epithelia. Sci Rep *9*, 6523. 10.1038/s41598-019-43002-2.

14. Tschaikner, P., Enzler, F., Torres-Quesada, O., Aanstad, P., and Stefan, E. (2020). Hedgehog and Gpr161: Regulating cAMP Signaling in the Primary Cilium. Cells *9*, E118. 10.3390/cells9010118.

15. Johnson, J.-L.F., and Leroux, M.R. (2010). cAMP and cGMP signaling: sensory systems with prokaryotic roots adopted by eukaryotic cilia. Trends Cell Biol *20*, 435–444. 10.1016/j.tcb.2010.05.005.

16. Bishop, G.A., Berbari, N.F., Lewis, J., and Mykytyn, K. (2007). Type III adenylyl cyclase localizes to primary cilia throughout the adult mouse brain. J Comp Neurol *505*, 562–571. 10.1002/cne.21510.

17. Mykytyn, K., and Askwith, C. (2017). G-Protein-Coupled Receptor Signaling in Cilia. Cold Spring Harb Perspect Biol, a028183. 10.1101/cshperspect.a028183.

18. Roa, J.N., Ma, Y., Mikulski, Z., Xu, Q., Ilouz, R., Taylor, S.S., and Skowronska-Krawczyk, D. (2021). Protein Kinase A in Human Retina: Differential Localization of Cβ, Cα, RIIα, and RIIβ in Photoreceptors Highlights Non-redundancy of Protein Kinase A Subunits. Frontiers in Molecular Neuroscience *14*.

19. Wen, X.-H., Dizhoor, A.M., and Makino, C.L. (2014). Membrane guanylyl cyclase complexes shape the photoresponses of retinal rods and cones. Front Mol Neurosci *7*, 45. 10.3389/fnmol.2014.00045.

20. Nguyen, P.A.T., Liou, W., Hall, D.H., and Leroux, M.R. (2014). Ciliopathy proteins establish a bipartite signaling compartment in a C. elegans thermosensory neuron. Journal of Cell Science *127*, 5317–5330. 10.1242/jcs.157610.

21. van der Burght, S.N., Rademakers, S., Johnson, J.-L., Li, C., Kremers, G.-J., Houtsmuller, A.B., Leroux, M.R., and Jansen, G. (2020). Ciliary Tip Signaling Compartment Is Formed and Maintained by Intraflagellar Transport. Current Biology *30*, 4299-4306.e5. 10.1016/j.cub.2020.08.032.

22. Lysko, D.E., Putt, M., and Golden, J.A. (2011). SDF1 Regulates Leading Process Branching and Speed of Migrating Interneurons. J. Neurosci. *31*, 1739–1745. 10.1523/JNEUROSCI.3118-10.2011.

23. Lysko, D.E., Putt, M., and Golden, J.A. (2014). SDF1 Reduces Interneuron Leading Process Branching through Dual Regulation of Actin and Microtubules. J. Neurosci. *34*, 4941–4962. 10.1523/JNEUROSCI.4351-12.2014.

24. Shelly, M., Cancedda, L., Lim, B.K., Popescu, A.T., Cheng, P., Gao, H., and Poo, M. (2011). Semaphorin3A Regulates Neuronal Polarization by Suppressing Axon Formation and Promoting Dendrite Growth. Neuron *71*, 433–446. 10.1016/j.neuron.2011.06.041.

25. Togashi, K., von Schimmelmann, M.J., Nishiyama, M., Lim, C.-S., Yoshida, N., Yun, B., Molday, R.S., Goshima, Y., and Hong, K. (2008). Cyclic GMP-gated CNG channels function in Sema3A-induced growth cone repulsion. Neuron *58*, 694–707. 10.1016/j.neuron.2008.03.017.

26. Polleux, F., Morrow, T., and Ghosh, A. (2000). Semaphorin 3A is a chemoattractant for cortical apical dendrites. Nature *404*, 567–573. 10.1038/35007001.

27. Smolenski, A. (2012). Novel roles of cAMP/cGMP-dependent signaling in platelets. Journal of Thrombosis and Haemostasis *10*, 167–176. 10.1111/j.1538-7836.2011.04576.x.

28. Zhu, K., Sun, Y., Miu, A., Yen, M., Liu, B., Zeng, Q., Mogilner, A., and Zhao, M. (2016). cAMP and cGMP Play an Essential Role in Galvanotaxis of Cell Fragments. J Cell Physiol *231*, 1291–1300. 10.1002/jcp.25229.

29. Averaimo, S., and Nicol, X. (2014). Intermingled cAMP, cGMP and calcium spatiotemporal dynamics in developing neuronal circuits. Front Cell Neurosci *8*. 10.3389/fncel.2014.00376.

30. Kobayashi, T., Nagase, F., Hotta, K., and Oka, K. (2013). Crosstalk between Second Messengers Predicts the Motility of the Growth Cone. Sci Rep *3*, 3118. 10.1038/srep03118.

31. Nishiyama, M., Hoshino, A., Tsai, L., Henley, J.R., Goshima, Y., Tessier-Lavigne, M., Poo, M., and Hong, K. (2003). Cyclic AMP/GMP-dependent modulation of Ca2+ channels sets the polarity of nerve growth-cone turning. Nature *423*, 990–995. 10.1038/nature01751.

32. Shelly, M., Lim, B.K., Cancedda, L., Heilshorn, S.C., Gao, H., and Poo, M. (2010). Local and Long-Range Reciprocal Regulation of cAMP and cGMP in Axon/Dendrite Formation. Science *327*, 547–552. 10.1126/science.1179735.

33. Mandal, S., Stanco, A., Buys, E.S., Enikolopov, G., and Rubenstein, J.L.R. (2013). Soluble guanylate cyclase generation of cGMP regulates migration of MGE neurons. J. Neurosci. *33*, 16897–16914. 10.1523/JNEUROSCI.1871-13.2013.

34. Bock, A., Annibale, P., Konrad, C., Hannawacker, A., Anton, S.E., Maiellaro, I., Zabel, U., Sivaramakrishnan, S., Falcke, M., and Lohse, M.J. (2020). Optical Mapping of cAMP Signaling at the Nanometer Scale. Cell *182*, 1519-1530.e17. 10.1016/j.cell.2020.07.035.

35. Brescia, M., and Zaccolo, M. (2016). Modulation of Compartmentalised Cyclic Nucleotide Signalling via Local Inhibition of Phosphodiesterase Activity. Int J Mol Sci *17*, 1672. 10.3390/ijms17101672.

36. Ros, O., Zagar, Y., Ribes, S., Baudet, S., Loulier, K., Couvet, S., Ladarre, D., Aghaie, A., Louail, A., Petit, C., et al. (2019). SponGee: A Genetic Tool for Subcellular and Cell-Specific cGMP Manipulation. Cell Reports *27*, 4003-4012.e6. 10.1016/j.celrep.2019.05.102.

37. Averaimo, S., Assali, A., Ros, O., Couvet, S., Zagar, Y., Genescu, I., Rebsam, A., and Nicol, X. (2016). A plasma membrane microdomain compartmentalizes ephrin-generated cAMP signals to prune developing retinal axon arbors. Nat Commun *7*, 12896. 10.1038/ncomms12896.

38. Lefkimmiatis, K., Moyer, M.P., Curci, S., and Hofer, A.M. (2009). "cAMP sponge": a buffer for cyclic adenosine 3', 5'-monophosphate. PLoS One *4*, e7649. 10.1371/journal.pone.0007649.

39. Kohen, R., Fashingbauer, L.A., Heidmann, D.E., Guthrie, C.R., and Hamblin, M.W. (2001). Cloning of the mouse 5-HT6 serotonin receptor and mutagenesis studies of the third cytoplasmic loop. Brain Res Mol Brain Res *90*, 110–117. 10.1016/s0169-328x(01)00090-0.

40. Zhang, J., Shen, C.-P., Xiao, J.C., Lanza, T.J., Lin, L.S., Francis, B.E., Fong, T.M., and Chen, R.Z. (2006). Effects of mutations at conserved TM II residues on ligand binding and activation of mouse 5-HT6 receptor. European Journal of Pharmacology *534*, 77–82. 10.1016/j.ejphar.2006.01.049.

41. Martini, F.J., Valiente, M., López Bendito, G., Szabó, G., Moya, F., Valdeolmillos, M., and Marín, O. (2009). Biased selection of leading process branches mediates chemotaxis during tangential neuronal migration. Development *136*, 41–50. 10.1242/dev.025502.

42. Konno, D., Shioi, G., Shitamukai, A., Mori, A., Kiyonari, H., Miyata, T., and Matsuzaki, F. (2008). Neuroepithelial progenitors undergo LGN-dependent planar divisions to maintain self-renewability during mammalian neurogenesis. Nat Cell Biol *10*, 93–101. 10.1038/ncb1673.

43. Ros, O., Baudet, S., Zagar, Y., Loulier, K., Roche, F., Couvet, S., Aghaie, A., Atkins, M., Louail, A., Petit, C., et al. (2020). SpiCee: A Genetic Tool for Subcellular and Cell-Specific Calcium Manipulation. Cell Reports *32*, 107934. 10.1016/j.celrep.2020.107934.

44. Jana, S.C. (2021). Centrosome structure and biogenesis: Variations on a theme? Semin Cell Dev Biol *110*, 123–138. 10.1016/j.semcdb.2020.10.014.

45. Hoppeler-Lebel, A., Celati, C., Bellett, G., Mogensen, M.M., Klein-Hitpass, L., Bornens, M., and Tassin, A.-M. (2007). Centrosomal CAP350 protein stabilises microtubules associated with the Golgi complex. Journal of Cell Science *120*, 3299–3308. 10.1242/jcs.013102.

46. Zaccolo, M., and Movsesian, M.A. (2007). cAMP and cGMP Signaling Cross-Talk. Circulation Research *100*, 1569–1578. 10.1161/CIRCRESAHA.106.144501.

47. Stierl, M., Stumpf, P., Udwari, D., Gueta, R., Hagedorn, R., Losi, A., Gärtner, W., Petereit, L., Efetova, M., Schwarzel, M., et al. (2011). Light modulation of cellular cAMP by a small bacterial photoactivated adenylyl cyclase, bPAC, of the soil bacterium Beggiatoa. J Biol Chem *286*, 1181–1188. 10.1074/jbc.M110.185496.

48. Viou, L., Launay, P., Rousseau, V., Masson, J., Pace, C., Adelstein, R.S., Ma, X., Jia, Z., Murakami, F., Barnier, J.-V., et al. (2020). PAK3 controls the tangential to radial migration switch of cortical interneurons by coordinating changes in cell shape and polarity. 2020.07.06.168179. 10.1101/2020.07.06.168179.

49. Li, G., Adesnik, H., Li, J., Long, J., Nicoll, R.A., Rubenstein, J.L.R., and Pleasure, S.J. (2008). Regional Distribution of Cortical Interneurons and Development of Inhibitory Tone Are Regulated by Cxcl12/Cxcr4 Signaling. J. Neurosci. *28*, 1085–1098. 10.1523/JNEUROSCI.4602-07.2008.

50. Sánchez-Alcañiz, J.A., Haege, S., Mueller, W., Pla, R., Mackay, F., Schulz, S., López-Bendito, G., Stumm, R., and Marín, O. (2011). Cxcr7 controls neuronal migration by regulating chemokine responsiveness. Neuron *69*, 77–90. 10.1016/j.neuron.2010.12.006.

51. Tiveron, M.-C., Rossel, M., Moepps, B., Zhang, Y.L., Seidenfaden, R., Favor, J., König, N., and Cremer, H. (2006). Molecular Interaction between Projection Neuron Precursors and Invading Interneurons via Stromal-Derived Factor 1 (CXCL12)/CXCR4 Signaling in the Cortical Subventricular Zone/Intermediate Zone. J. Neurosci. *26*, 13273–13278. 10.1523/JNEUROSCI.4162-06.2006.

52. Sessa, A., Mao, C.-A., Colasante, G., Nini, A., Klein, W.H., and Broccoli, V. (2010). Tbr2-positive intermediate (basal) neuronal progenitors safeguard cerebral cortex expansion by controlling amplification of pallial glutamatergic neurons and attraction of subpallial GABAergic interneurons. Genes Dev *24*, 1816–1826. 10.1101/gad.575410.

53. Hu, L., Wang, B., and Zhang, Y. (2017). Serotonin 5-HT6 receptors affect cognition in a mouse model of Alzheimer's disease by regulating cilia function. Alzheimer's Research & Therapy *9*, 76. 10.1186/s13195-017-0304-4.

54. Polito, M., Klarenbeek, J., Jalink, K., Paupardin-Tritsch, D., Vincent, P., and Castro, L.R.V. (2013). The NO/cGMP pathway inhibits transient cAMP signals through the activation of PDE2 in striatal neurons. Front Cell Neurosci *7*, 211. 10.3389/fncel.2013.00211.

55. Clement, D.L., Mally, S., Stock, C., Lethan, M., Satir, P., Schwab, A., Pedersen, S.F., and Christensen, S.T. (2013). PDGFRα signaling in the primary cilium regulates NHE1-dependent fibroblast migration via coordinated differential activity of MEK1/2–ERK1/2–p90RSK and AKT signaling pathways. Journal of Cell Science *126*, 953–965. 10.1242/jcs.116426.

56. Lee, M.N., Song, J.H., Oh, S.-H., Tham, N.T., Kim, J.-W., Yang, J.-W., Kim, E.-S., and Koh, J.-T. (2020). The primary cilium directs osteopontin-induced migration of mesenchymal stem cells by regulating CD44 signaling and Cdc42 activation. Stem Cell Research *45*, 101799. 10.1016/j.scr.2020.101799.

57. Mansini, A.P., Peixoto, E., Jin, S., Richard, S., and Gradilone, S.A. (2019). The chemosensory function of primary cilia regulates cholangiocyte migration, invasion and tumor growth. Hepatology *69*, 1582–1598. 10.1002/hep.30308.

58. Kurelic, R., Krieg, P.F., Sonner, J.K., Bhaiyan, G., Ramos, G.C., Frantz, S., Friese, M.A., and Nikolaev, V.O. (2021). Upregulation of Phosphodiesterase 2A Augments T Cell Activation by Changing cGMP/cAMP Cross-Talk. Frontiers in Pharmacology *12*.

59. Pietrobon, M., Zamparo, I., Maritan, M., Franchi, S.A., Pozzan, T., and Lodovichi, C. (2011). Interplay among cGMP, cAMP, and Ca2+ in Living Olfactory Sensory Neurons In Vitro and In Vivo. J. Neurosci. *31*, 8395–8405. 10.1523/JNEUROSCI.6722-10.2011.

60. Stoufflet, J., Chaulet, M., Doulazmi, M., Fouquet, C., Dubacq, C., Métin, C., Schneider-Maunoury, S., Trembleau, A., Vincent, P., and Caillé, I. (2020). Primary cilium-dependent cAMP/PKA signaling at the centrosome regulates neuronal migration. Sci Adv *6*, eaba3992. 10.1126/sciadv.aba3992.

61. Terrin, A., Monterisi, S., Stangherlin, A., Zoccarato, A., Koschinski, A., Surdo, N.C., Mongillo, M., Sawa, A., Jordanides, N.E., Mountford, J.C., et al. (2012). PKA and PDE4D3 anchoring to AKAP9 provides distinct regulation of cAMP signals at the centrosome. J Cell Biol *198*, 607–621. 10.1083/jcb.201201059.

62. Stumm, R., Kolodziej, A., Schulz, S., Kohtz, J.D., and Höllt, V. (2007). Patterns of SDF-1α and SDF-1γ mRNAs, migration pathways, and phenotypes of CXCR4-expressing neurons in the developing rat telencephalon. Journal of Comparative Neurology *502*, 382–399. 10.1002/cne.21336.

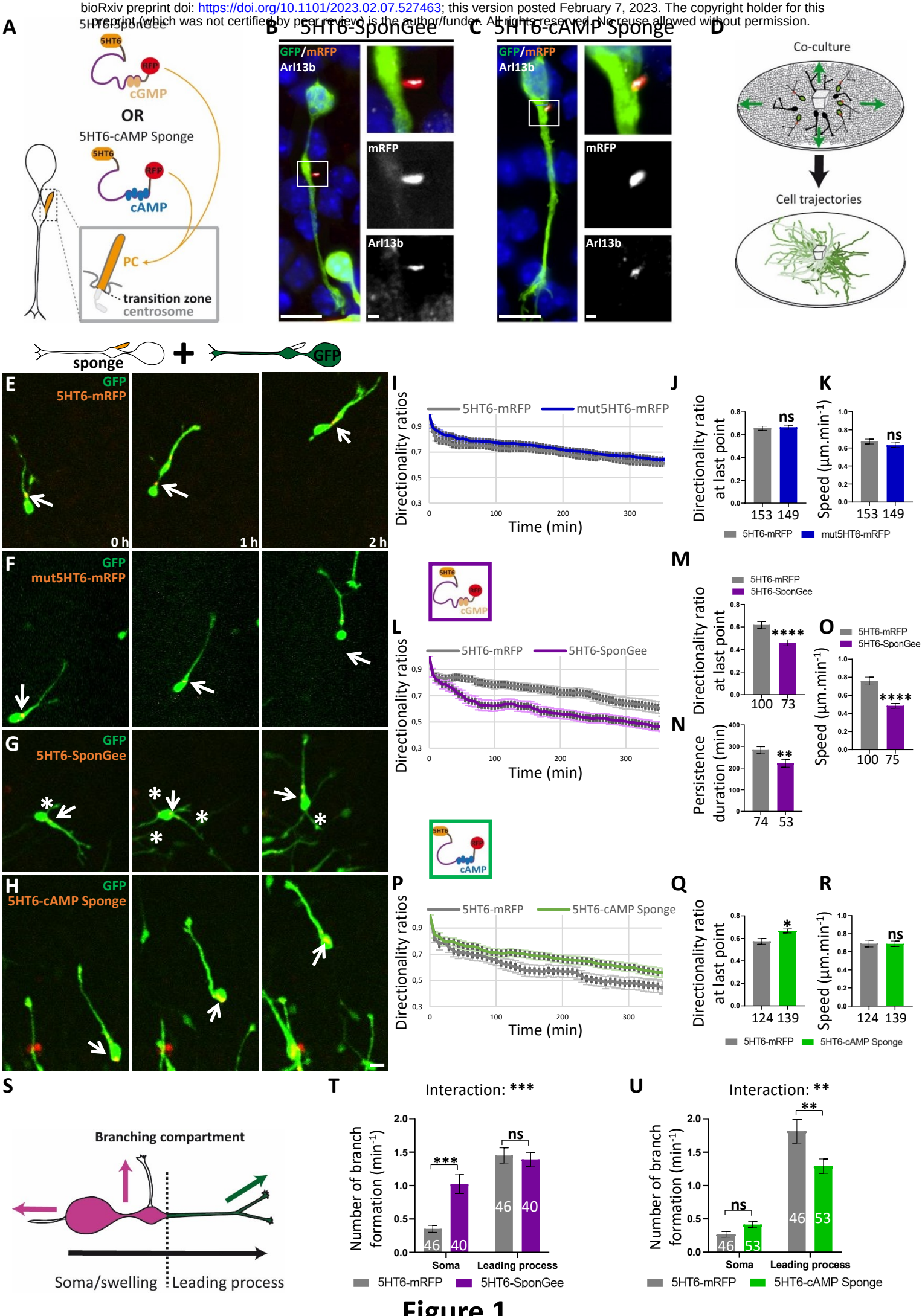

Figure 1

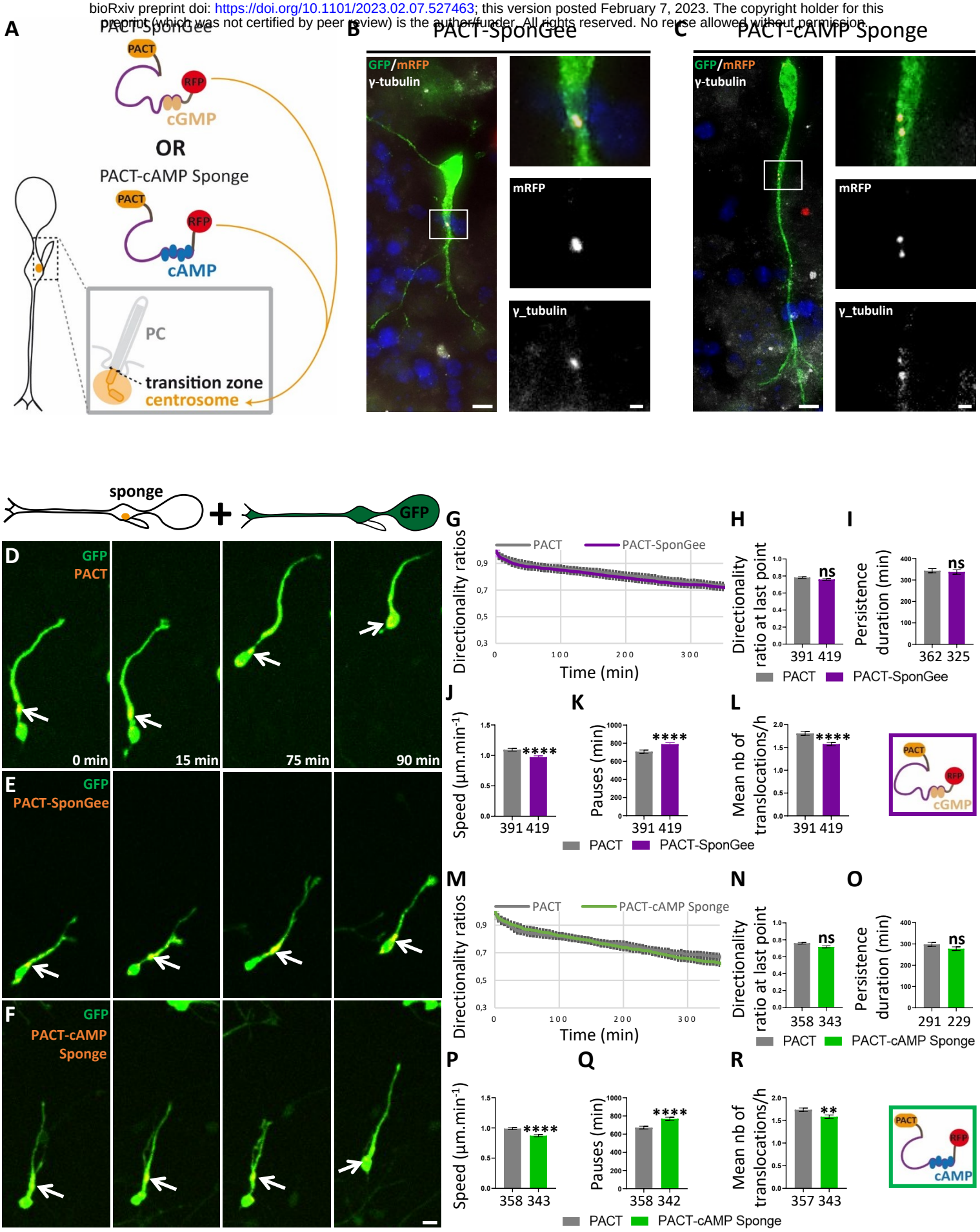

Figure 2

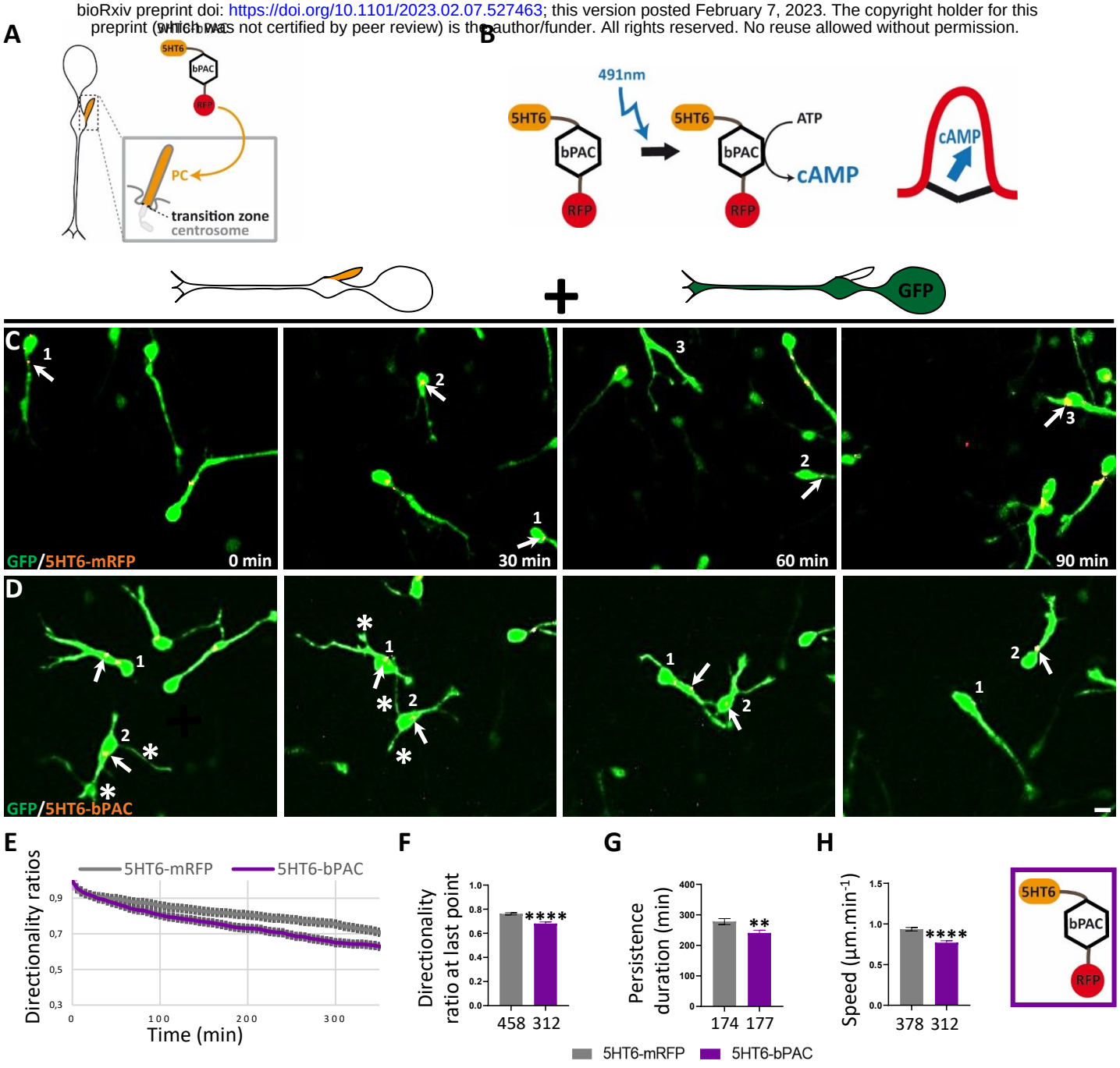

Figure 3

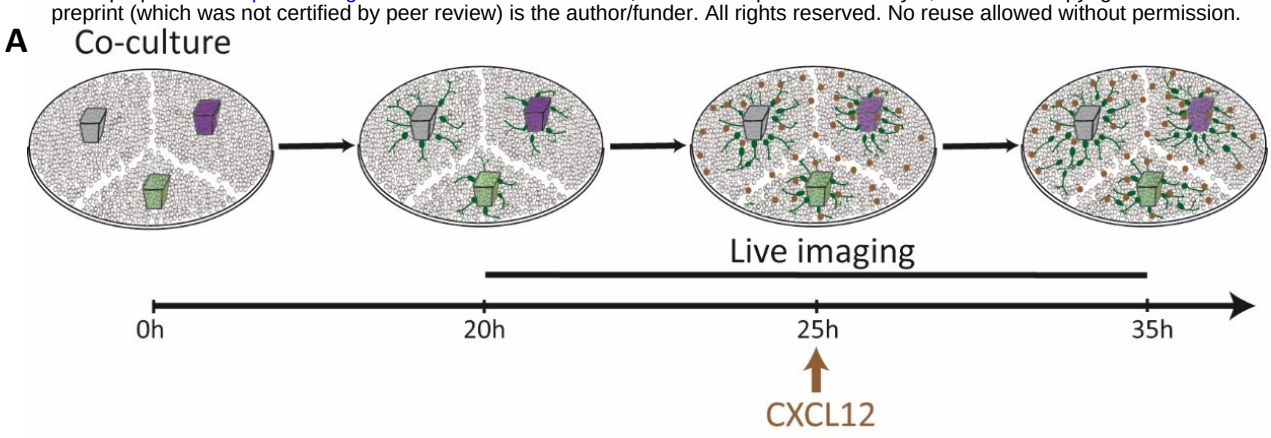

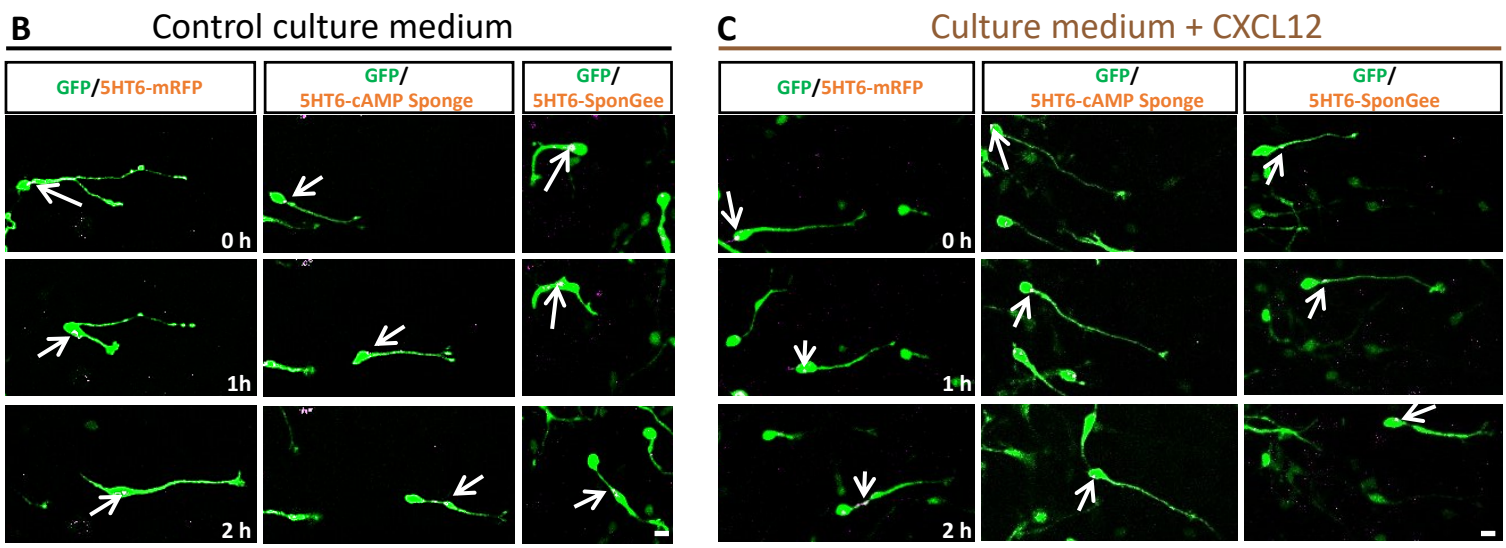

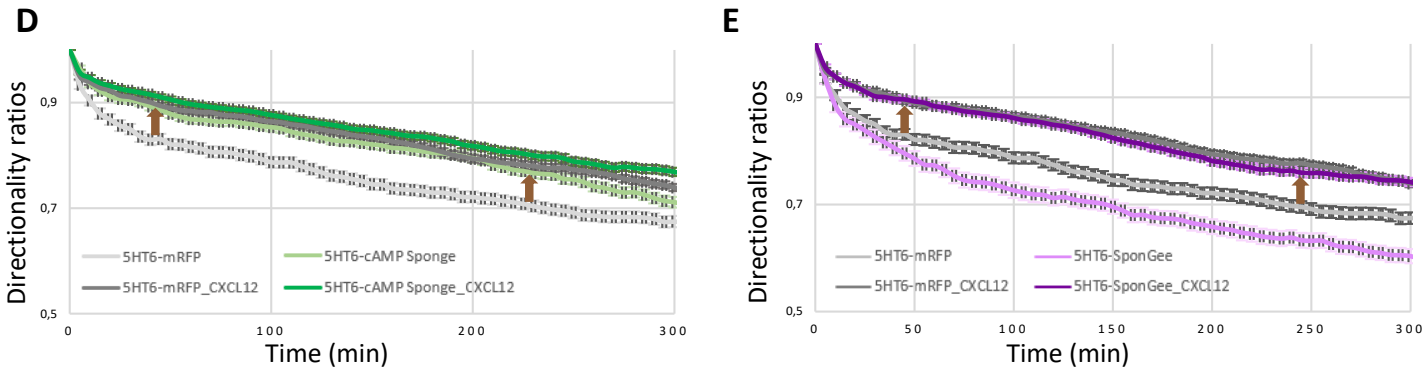

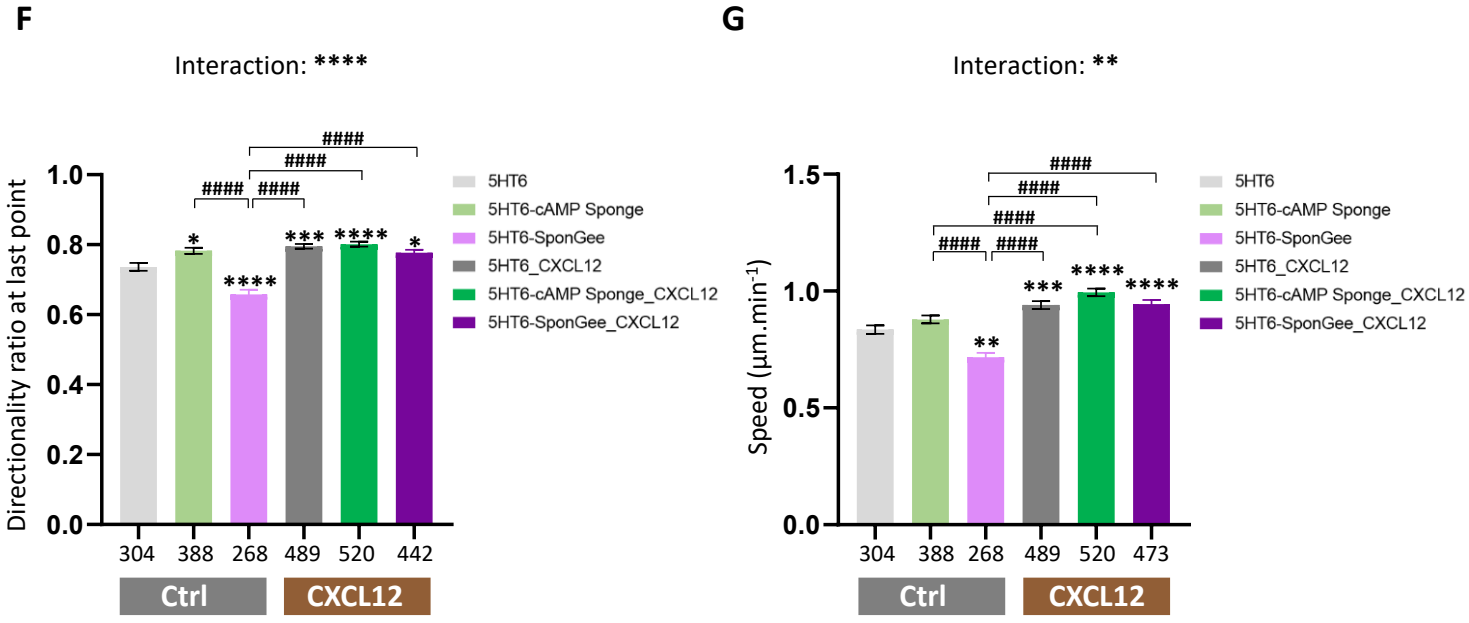

Figure 4

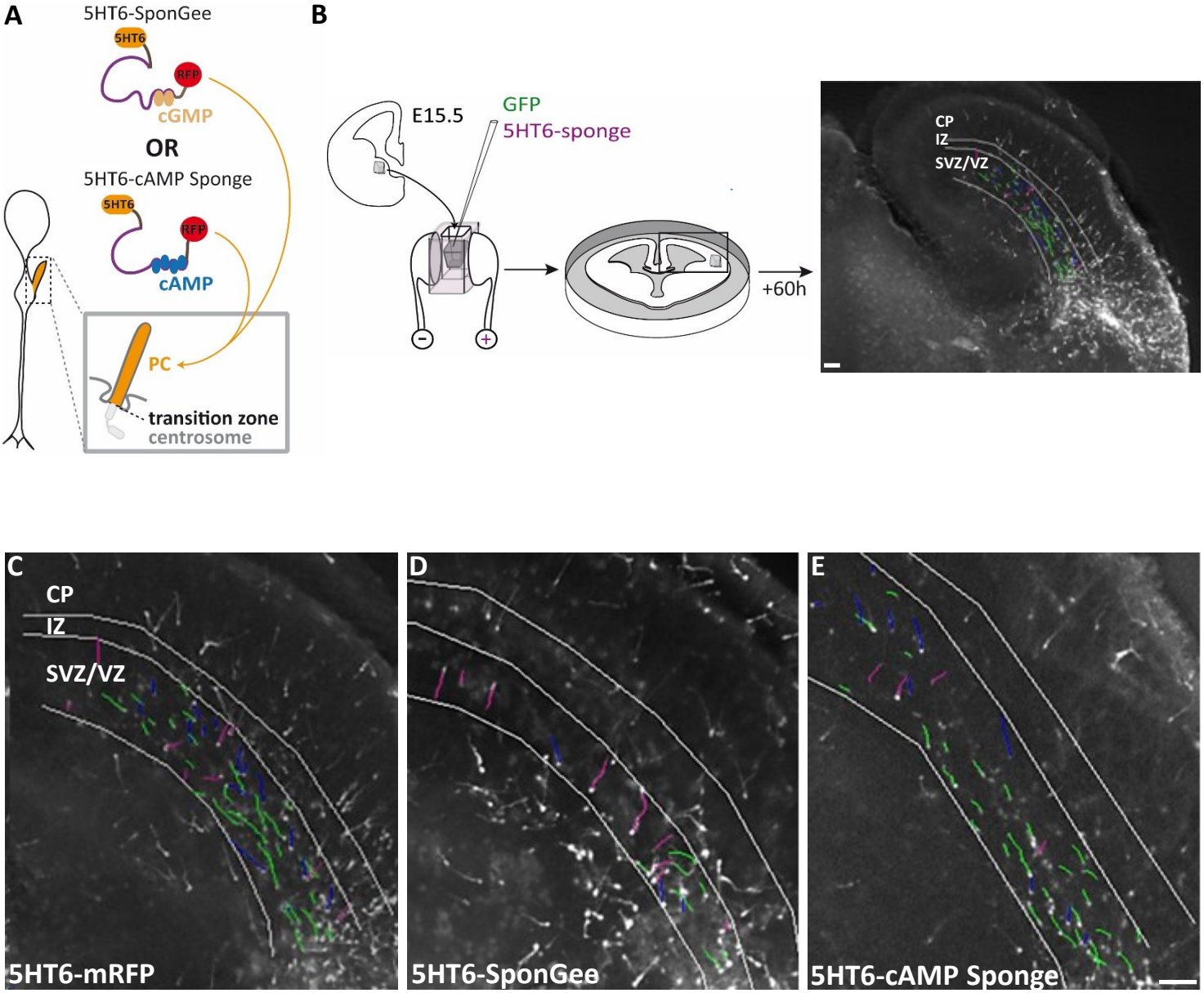

Figure 5

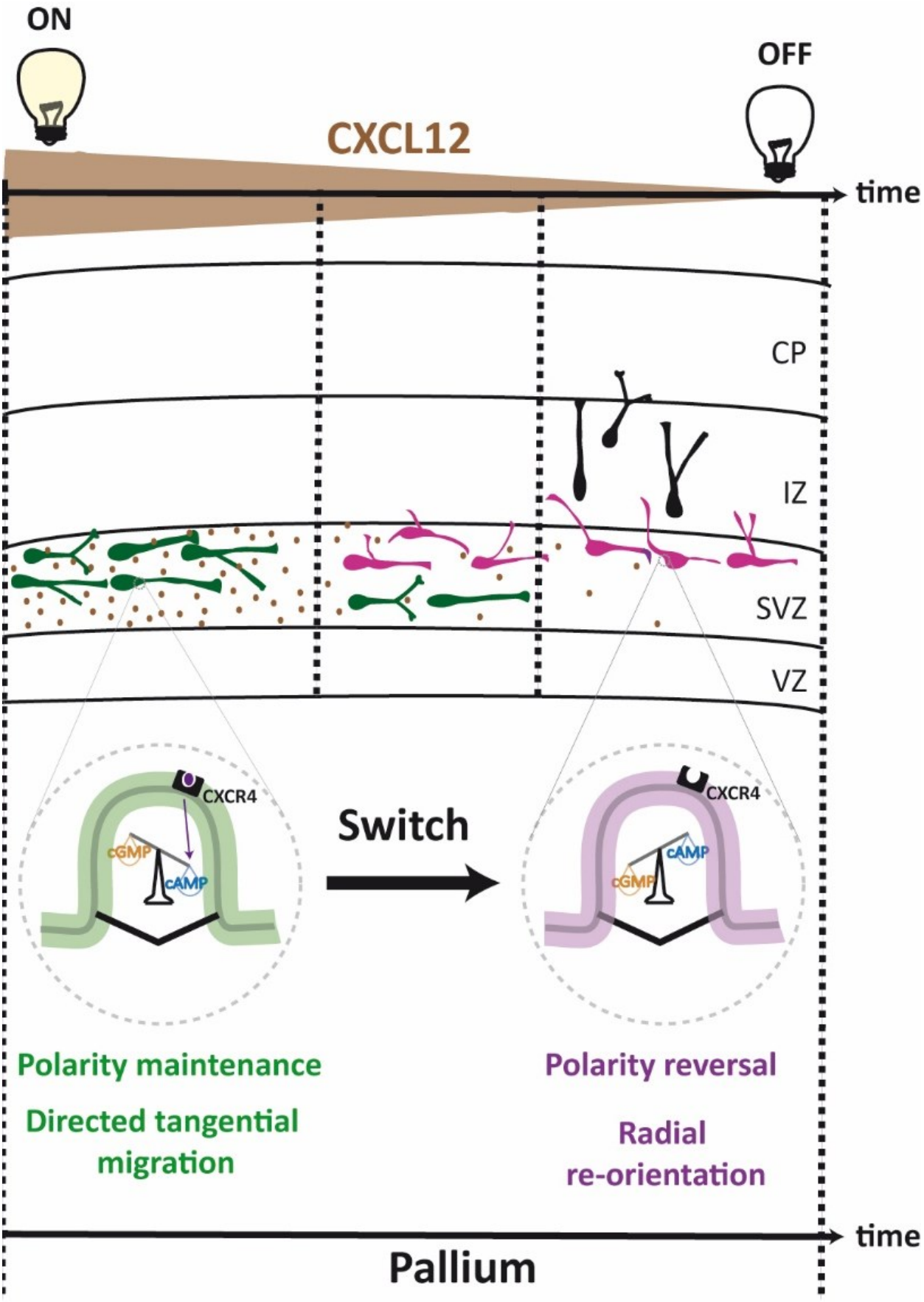

Figure 6

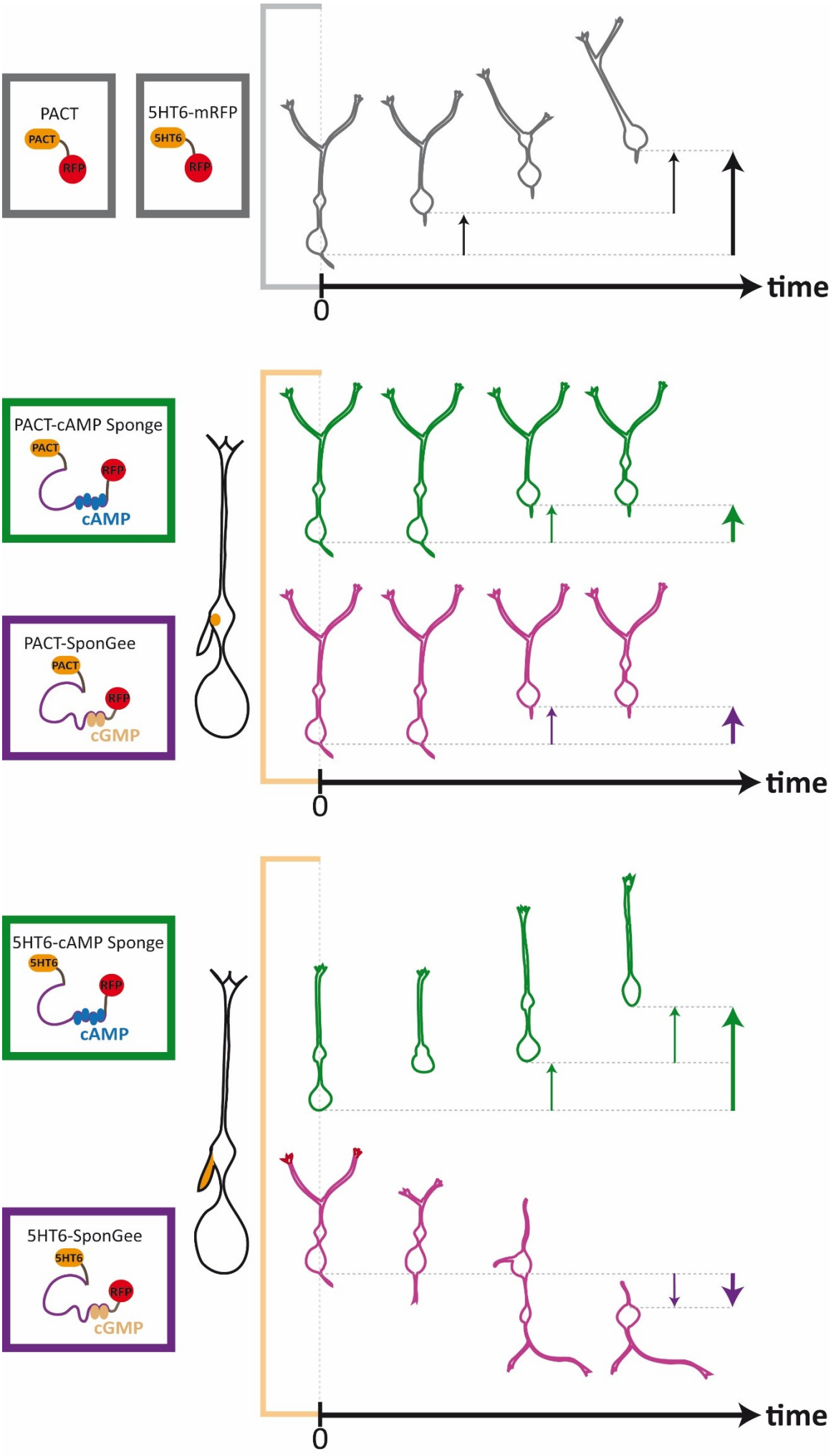

Figure S1

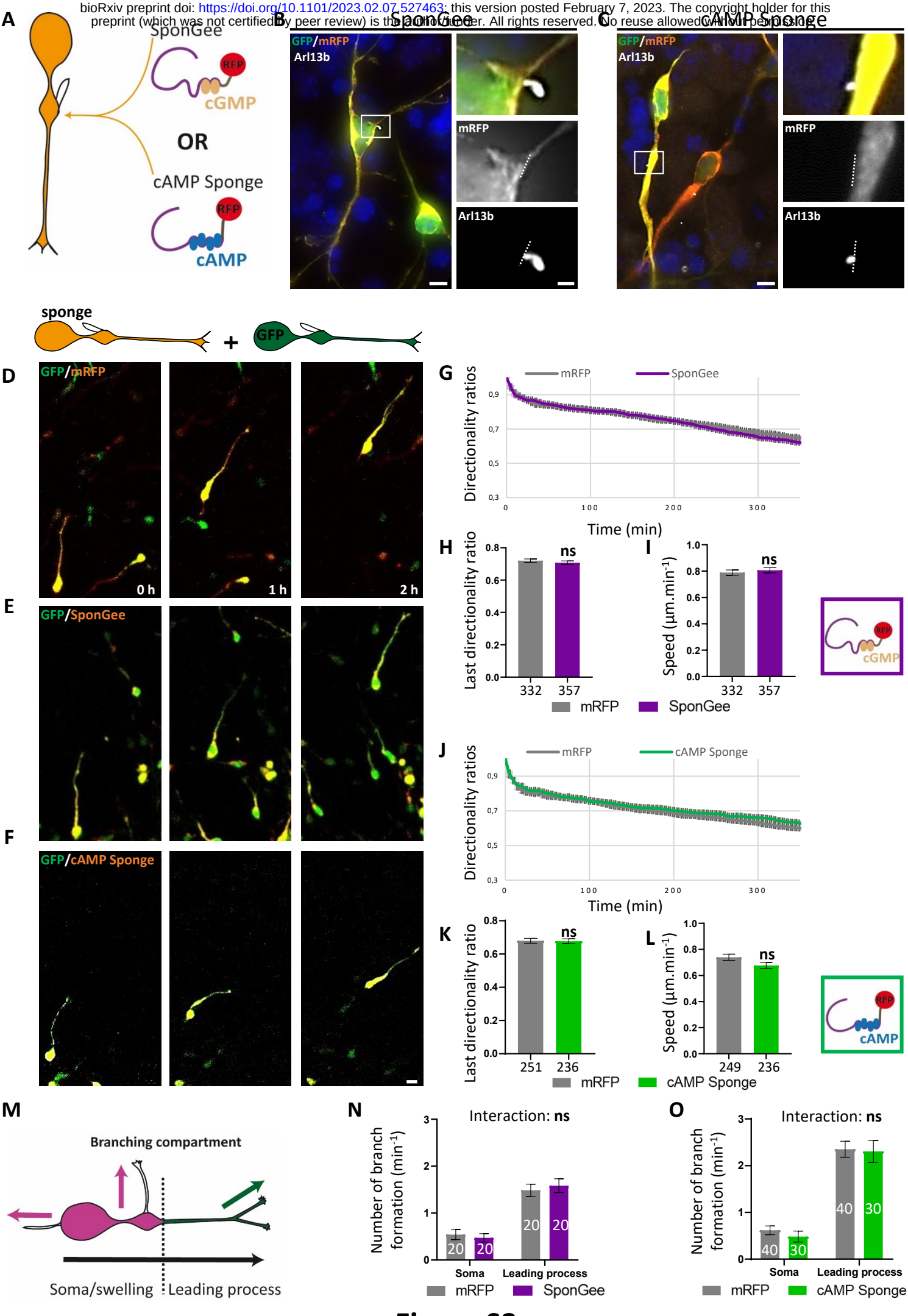

Figure S2